On the effect of negative triangularity on Ion Temperature Gradient turbulence in tokamaks

Gabriele Merlo, Mattia Dicorato, Bryce Allen, Tilman Dannert, Kai Germaschewski, Frank Jenko

On the effect of negative triangularity on Ion Temperature Gradient turbulence in tokamaks

Gabriele Merlo
Oden Institute for Computational Engineering and Sciences, The University of Texas at Austin, Austin, TX 78712, USA

Mattia Dicorato
Aix-Marseille Université, CNRS, PIIM UMR 7345, Marseille, France and CEA, IRFM, F-13108 Saint Paul Lez Durance, France

Bryce Allen
Department of Computer Science, The University of Chicago, Chicago, Illinois 60637, USA and Computational Science Division, Argonne National Laboratory, Lemont, Illinois 60439, USA

Tilman Dannert
Max Planck Computing and Data Facility, 85748 Garching, Germany

Kai Germaschewski
Department of Physics and Space Science Center, University of New Hampshire , Durham, New Hampshire 03824, USA

Frank Jenko
Oden Institute for Computational Engineering and Sciences, The University of Texas at Austin, Austin, TX 78712, USA
Institute for Fusion Studies, The University of Texas at Austin, Austin, TX 78712, USA and Max-Planck-Institut für Plasmaphysik, Boltzmannstr. 2, D-85748 Garching, Germany

(*gmerlo@oden.utexas.edu)

(Dated: September 11, 2023)

Abstract

Considering the same magnetic equilibrium and plasma conditions as in [Duff et al. Phys.Plasmas 29, 012303(2022)], we perform linear and nonlinear simulations of electrostatic ion temperature gradient turbulence investigating the role of triangularity δ. Differently from what was previous reported, we find that triangularity increases the transport level regardless of its sign, but more strongly when δ is positive. For the case analyzed, we identify the shear of triangularity as the critical parameter determining the transport level, indicating that even in the local limit negative triangularity can reduce the transport efficiently, suggesting that confinement improvement can also be expected for larger devices.

I. INTRODUCTION

ITER and future fusion reactors are expected to exploit High-confinement (H-mode) regimes [1] in order to reach plasma core conditions sufficient to obtain a positive net production of energy. These regimes, which rely on sustaining a narrow edge transport barrier, have however also widely recognized disadvantages. The occurrence of Edge-Localized Modes (ELMs) is perhaps the most critical one. These violent bursts of energy are detrimental to the machine integrity and, while they are tolerable in current experiments, they are not acceptable for a fusion reactor. This motivated vigorous research on ways of limiting, or at least controlling, these dangerous events. Along these lines, an alternative approach appears to be provided by negative triangularity plasmas, which are experimentally found to be able to provide H-mode confinement quality without the need of an edge transport barrier, therefore avoiding the ELM issue altogether. First explored in the Tokamak à Configuration Variable (TCV) [2], negative triangularity has successfully been investigated also in the DIII-D tokamak[3]. The reader is referred to Ref. [4] for a review of negative triangularity experiments.

Following these experimental observations, a number of works have been reported, addressing the origin of the confinement improvement on the basis of gyrokinetic simulations of microturbulence [5–12]. Most of the cases considered successfully reproduced the experimentally observed confinement improvement, which is understood as a result of Trapped Electron Mode stabilization, even though parameters regimes where negative triangularity is expected not to yield an improvement have also been identified [13].

Whether the turbulence reduction persists in different turbulence regimes, notably Ion Temperature Gradient (ITG) dominated plasmas, remains an open question. Different results have been found in this regard, in particular Refs. [8, 13, 14] indicate that negative triangularity can be beneficial also for ITG conditions, whereas [15] does not find any significant difference when investigating plasmas shaped with extreme positive or negative triangularity. This work, based on extensive nonlinear simulations, re-examines the issue of the impact of triangularity on electrostatic ITG turbulence modeled with adiabatic electrons. Considering the same set-up as the one described in [15], we find that negative δ can have a substantial effect of transport, reducing the fluxes by up to more than a factor of two. The stabilization is observed both linearly and nonlinearly, and in agreement with Refs. [15] and [16] we obtain that the plasma shaping influences the behavior of zonal flows. A reduction of the zonal flow shearing rate with triangularity is found regardless of

its sign but because of the higher linear growth rates when triangularity is positive, the transport is lower for negative triangularity. We have analyzed the dependence of the transport with other shaping parameters, and identify the triangularity shear as a key parameter. A large radial variation of triangularity amplifies the difference between shapes, whereas a much smaller value can nullify the differences. These results indicate that, provided the plasma geometry is properly optimized, negative triangularity can be beneficial also for ITG dominated regimes and that, even if such confinement may be localized over a small fraction of the minor radius, it can be substantial. Furthermore, even if δ rapidly goes to zero towards the magnetic axis, a $\delta < 0$ configuration can result in transport suppression in the near edge region, without needing nonlocal effects and thus also for large devices.

The remainder of the paper is organized as follows. Section II and III present the numerical methods used for the analysis and provide the details of the magnetic geometry. Linear results are discussed in Sec. IV and nonlinear in V. A summary and conclusions are presented in Sec. VI.

II. NUMERICAL METHODS

The main computational tool used in this work is the gyrokinetic GENE code [17]. GENE solves the gyrokinetic equation[18] using a field aligned coordinate system (x,y,z) to discretize the configuration space, while $(v_\parallel,\mu)$ are used as velocity variables. Here x stands for the radial, y for the binormal and z for the parallel direction. The variable $\mu = mv_\perp^2/2B$ represents the magnetic moment, while $v_\parallel$ and $v_\perp$ the components of velocity respectively parallel and perpendicular to the magnetic field; m is the mass of the particle and B the local magnitude of the magnetic equilibrium field $\mathbf{B}$. All simulations are performed in the local (flux-tube) limit, in which periodic boundary conditions are employed in both x and y directions.

The magnetic geometry is specified via a standard Miller parametrization [19]. Thus, a flux-surface is parametrized on a poloidal plane $\varphi = \text{const}$ in cylindrical coordinates (R,Z,φ) as

$$R(r,\theta) = R_{geom}(r) + r\cos\{\theta + \arcsin[\delta(r)\sin\theta]\}, \tag{1}$$

$$Z(r,\theta) = Z_{geom}(r) + \kappa(r) r \sin[\theta + \zeta(r)\sin(2\theta)], \tag{2}$$

where the elongation κ, triangularity δ and squareness ζ have been introduced. Here r is the geometric minor radius $r = (R_{max} - R_{min})/2$.

III. ION TEMPERATURE GRADIENT TURBULENCE

We simulate the same case used by Duff *et al.* [15], that is the Waltz standard case modified to include triangularity. We report the simulation set-up for completeness. We consider a flux-surface with $r/a = 0.5$ and $R/a = 3$, safety factor $q = 2$ and magnetic shear $s = r/q\ dq/dr = 1$. Triangularity is varied within the range ± 0.8, while elongation is set to $\kappa = 1$ and squareness to $\zeta = 0$. The additional radial derivatives of the shaping parameters appearing in (1) and (2) are evaluated accordingly to

$$s_\kappa = \frac{r}{\kappa}\frac{\partial \kappa}{\partial r} = \frac{\kappa - 1}{\kappa}, \tag{3}$$

$$s_\delta = \frac{r}{\sqrt{1-\delta^2}}\frac{\partial \delta}{\partial r} = \frac{\delta}{\sqrt{1-\delta^2}}, \tag{4}$$

$$\frac{\partial R_{geom}}{\partial r} = 0, \tag{5}$$

$$Z_{geom}(r) = \frac{\partial Z_{geom}}{\partial r} = 0. \tag{6}$$

The plasma gradients are taken as $a/L_{T_i} = 4$ and a/L_n=1. Electrons are adiabatic and with the same temperature as the main ions. Unless differently stated, simulation use the same resolution as Duff *et al*, which we have verified yields numerically converged results.

IV. LINEAR RESULTS

The linear stability analysis is summarized in Figure 1, where we plot growth rate and frequency of the most unstable mode, neglecting the effect of a finite ballooning angle χ_0 (i.e. we assume $\chi_0 = 0$). In agreement with previous results [13, 15], we obtain that the growth rate peaks for a finite positive triangularity. To increase the confidence in our results we also show in subplots b and c growth rates and frequencies for $\delta = \pm 0.8$ computed with the GKW code [20], which agree excellently with GENE ones. Note that in this case we plot the results as a function of the equivalent poloidal mode number $nq\rho_s/a$ to facilitate the code comparison [21]. The dependence of γ is nonetheless a complex function of both δ and k_y. Specifically, we observe that for $k_y\rho_s > 0.2$ the ratio $\gamma(k_y, -|\delta|)/\gamma(k_y, +|\delta|)$ is always smaller than one and diminishes as triangularity is increased in magnitude, i.e. negative triangularity is linearly more stable. For $k_y\rho_s < 0.1$ ($nq\rho_s/a < 0.05$) the ratio is inverted with positive triangularity more stable as can be seen in Figs. 1.b and 1.c.

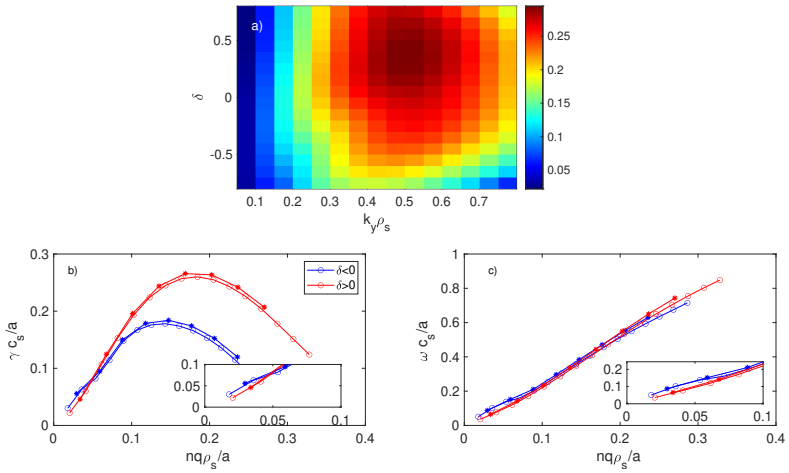

FIG. 1. (a) Linear growth rates as a function of the wave number $k_y\rho_s$ and triangularity δ. (b,c) Same results for $\delta = \pm 0.8$, circles indicate results obtained with the GENE code, stars GKW; in this case we plot them as a function of the equivalent poloidal mode number $nq\rho_s/a$. Insets show zooms at large wavenumbers where the behavior is flipped.

In order to try to better understand how the geometry affects the linear behavior of the microinstability, we can examine in more detail the various terms appearing in the gyrokinetic equation. The electrostatic linear δf collisionless gyrokinetic Vlasov equation for the perturbed ion distribution function f considering adiabatic electrons, can be written (following the GENE representation [22]) as

$$\frac{\partial f}{\partial t} = -\left\{\left[\omega_n + \omega_T\left(\frac{v_\parallel^2+\mu B_0}{T_0}-\frac{3}{2}\right)\right]F_0 + \frac{\mu B_0+2v_\parallel^2}{T_0 B_0}K_y F_0\right\}\frac{\partial \bar{\phi}}{\partial y} \tag{7}$$

$$-\frac{\mu B_0+2v_\parallel^2}{T_0 B_0}F_0 K_x\frac{\partial \bar{\phi}}{\partial x} - \frac{\mu B_0+2v_\parallel^2}{qB_0}K_x\frac{\partial f}{\partial x} \tag{8}$$

$$-\frac{\mu B_0+2v_\parallel^2}{qB_0}K_y\frac{\partial f}{\partial y} \tag{9}$$

$$-v_T\frac{1}{JB_0}v_\parallel\left(\frac{\partial f}{\partial z}+\frac{q}{T_0}F_0\frac{\partial \bar{\phi}}{\partial z}\right) \tag{10}$$

$$+\frac{v_T}{2}\frac{1}{JB_0}\mu\frac{\partial B_0}{\partial z}\frac{\partial f}{\partial v_\parallel} \tag{11}$$

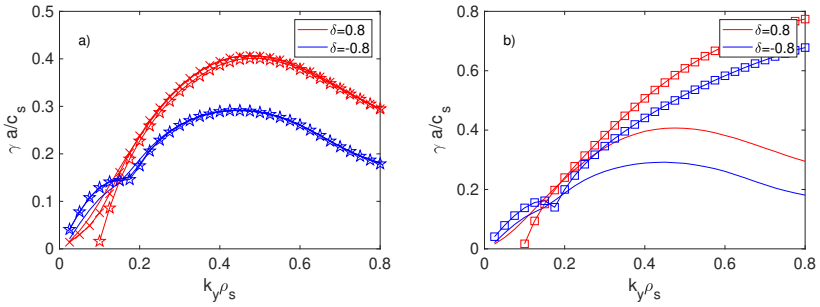

FIG. 2. Linear growth rates for $a/L_n = 1$, $a/L_T = 6$ n (red for $\delta = 0.8$ and blue for $\delta = -0.8$). Panel a) compares the complete gyrokinetic results (solid lines) to the results obtained considering only the mode $k_x = 0$ (crosses) and dropping the mirror force term in Eq. (11) (stars). Panel b) compares instead with the results obtained assuming $J_0 = 1$ (squares).

where $\bar{\phi} = J_0\phi$ the gyroaveraged potential (obtained from the quasineutrality equation), F_0 the background distribution function (a local Maxwellian is assumed here) and ω_n and ω_T the logarithm gradients of density and temperature. Equation (11) determines the complete three dimensional structure of the eigenfunction together with growth rates and frequencies. The effect of the magnetic geometry stems from the curvature terms

$$K_x = -\left(g^{xy}g^{yz} - g^{yy}g^{xz}\right)\frac{\partial B_0}{\partial z}, \tag{12}$$

$$K_y = \left(g^{xx}g^{yy} - \left(g^{xy}\right)^2\right)\frac{\partial B_0}{\partial x} - \left(g^{xx}g^{yz} - g^{xy}g^{xz}\right)\frac{\partial B_0}{\partial z}, \tag{13}$$

which are responsible for the stabilization that can be observed with negative δ. Here g^{ij} are the metric elements associated to GENE's coordinate system (we refer the reader to e.g. Ref. [22] for further details). Given that we are limiting to ITG turbulence, Equation (11) can be simplified considering $k_x = 0$ and neglecting the mirror force (last term in Eq. (11)) whereas all other terms, including the parallel variation of J_0 must be retained. An example is show in Figure 2, where we compare the results obtained from the full Vlasov system to simplifications. Neglecting the FLR effects, i.e. assuming $J_0 = 1$ as commonly done when deriving analytic local dispersion relations, is a too crude approximation that reduces the differences between positive and negative δ growth rates. As expected, the stabilization results from the complex spatial effect of curvature and parallel dynamics, which in turn determine also the eigenfunction, as shown in Figure 3. At

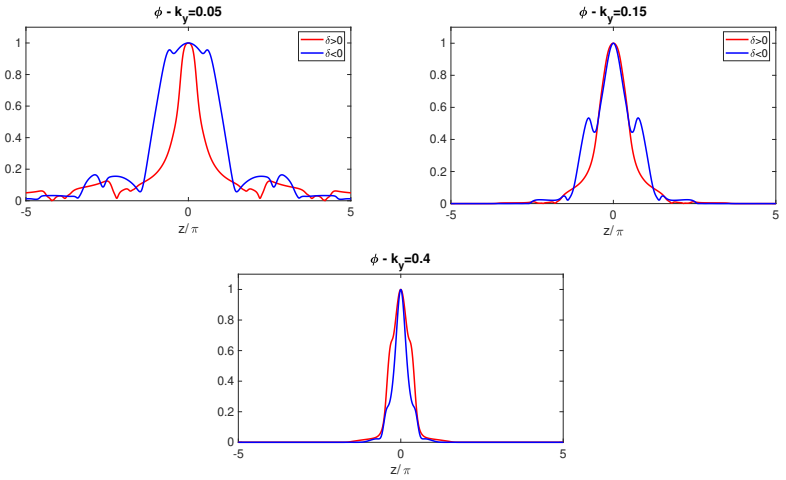

FIG. 3. Linear eigenfunction for from left to right k_y=0.05, 0.05 and 0.4. Red for $\delta = 0.8$ and blue for $\delta = -0.8$.

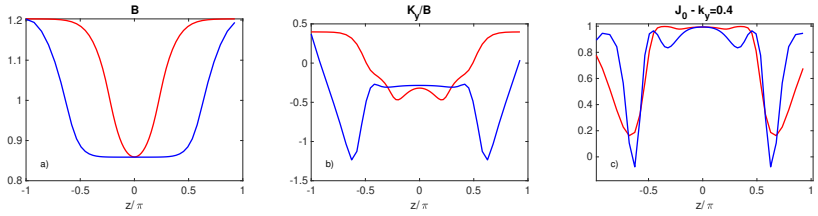

FIG. 4. Essential geometric parameters determining the different linear stability with triangularity; from left to right, a) magnetic field B, b) the binormal curvature K_y and the Bessel function J_0 evaluated for $k_y = 0.4$ responsible for FLR effects.

very low k_y, where the FLR stabilization is small, negative triangularity shows a slightly higher growth rate (more clearly visible when we consider only the $k_x = 0$ mode), which is caused by the broader region of bad curvature (see Fig. 4.b) whereas as k_y increases FLR effects become more important and are more stabilizing for $\delta < 0$ (Fig. 4.c). As we will show later on, the derivative of triangularity appears to play a very important role, with a finite s_δ causing significantly larger fluxes when $\delta > 0$ compared to $s_\delta < 0$. Thus, the sake of completeness, we compare in Figure

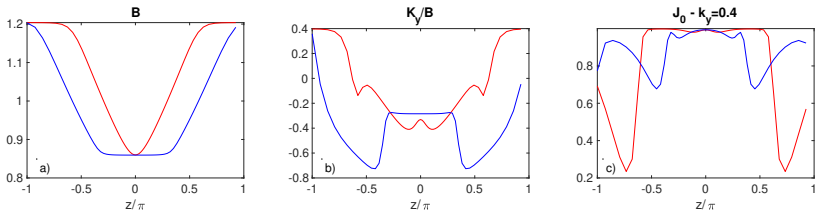

FIG. 5. Same as Fig. 4 but showing quantities for the case with $s_\delta = 0$.

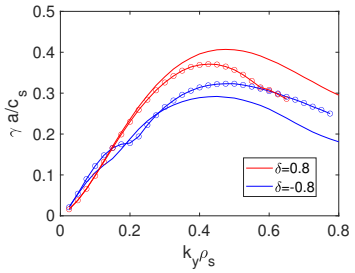

FIG. 6. Growth rates obtained with (solid lines) finite and (circles) zero triangularity shear.

6 the growth rates obtained with finite and the extreme case of zero triangularity shear. In this complicated (and dependent on the details of the magnetic geometry) picture, s_δ affects the linear stability by mostly modifying the metric element g^{yy}, in turn determining the magnitude of FLR effects (see Figure 5.c) and thus effectively reducing the difference $\delta > 0$ vs. $\delta < 0$ when s_δ is reduced to zero for modes $k_y \sim 0.3 - 0.6$. FLR effects alone are however not able to explain entirely the different linear behavior. An example, obtained increasing the safety factor q, is shown in Figure 7. The observed difference $\delta > 0$ to $\delta < 0$ for the base $q = 2$ case is in this case significantly reduced without modifying the binormal curvature or the FLR magnitude, but by modifying the parallel dynamics.

V. NONLINEAR RESULTS

Nonlinear simulations results varying δ are summarized in Figure 8. Here we plot the heat flux, time averaged over the nonlinear saturated state, in GyroBohm units $Q_{GB} = c_s p_i (\rho_s/a)^2$, with p_i

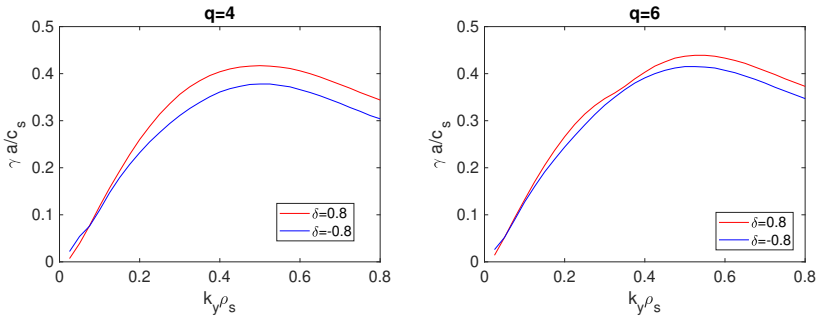

FIG. 7. Linear growth rates as a function of the wave number $k_y\rho_s$ and triangularity δ for different values of the safety factor q (cf. Fig. 1).

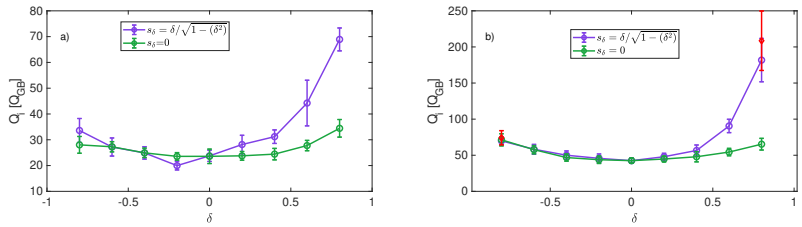

FIG. 8. Simulated ion heat flux in GyroBohm Units as a function of triangularity δ (a) for the base parameter set and $b)$ for increased ITG drive. Red diamonds indicate results (at finite s_δ obtained with the GKW code.

the ion pressure, neglecting the variation of the flux surface area S as a function of triangularity. Said variation is not negligible, with S decreasing roughly by 20% when going from the extreme negative to extreme positive δ, but does not change the qualitative trends. Error bars on the mean flux value are evaluated as the standard variation of the mean computed over disjoint intervals (each 100 a/c_s) of the simulated time trace. In Figure 8.a, as δ varies, we observe the presence of a minimum of fluxes for $\delta = -0.2$, with fluxes rapidly increasing, much more for positive δ, when the magnitude of triangularity is large. We point out that the exact location of the minimum as a function of δ is not precise (the time averaged transport values are characterized by at least a 10% uncertainty due to the bursty behavior of fluxes which affects the location of the minimum)

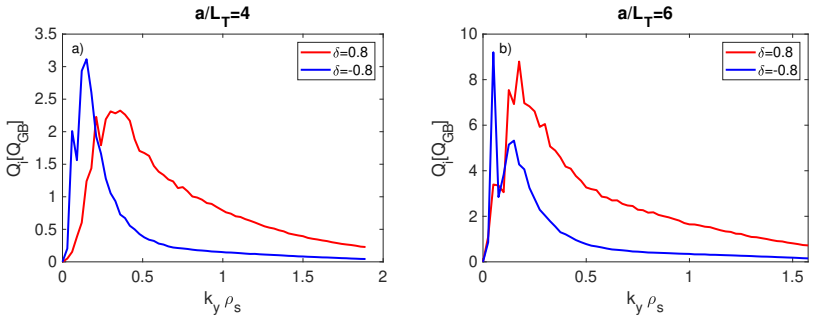

FIG. 9. Simulated flux spectra for (a) $a/L_{T_i} = 4$ and (b) $a/L_{T_i} = 6$ for $\delta = \pm 0.8$ (red positive δ, blue negative).

but is not particularly relevant here. The general trend of fluxes with increasing $|\delta|$ is however robust, and appears even more clearly for increased ITG drive, see Figure 8.b, where we depict the results obtained with $a/L_n = 1$ and $a/L_T = 6$ showing the same behavior. We also note that result obtained when neglecting the radial variation of triangularity ($s_\delta = 0$) are much less affected by δ variations, implying that the exact effect of δ on ITG strongly depends on the details of the magnetic geometry. We will discuss this aspect in the following. Finally, we point out that such effect of triangularity is in agreement with other works that focused on ITG turbulence modelled with adiabatic electrons, [13, 14], is clearly different from what reported by Duff *et al.*. The discrepancy between the results appears to be caused by a modification of the GENE coordinate system [23] used in Ref. [15], which we cannot reproduce. Once again, to strengthen our results, we have also performed a few additional runs with the GKW code, which agree well with GENE's ones.

Figure 9 shows the flux spectra, as a function of the binormal wavenumber for the extreme values of triangularity. For both values of temperature gradient we find that the wavenumber contributing most to the transport k_y^{max} is shifted towards lower values when $\delta < 0$ and that the reduction of transport originates from an overall reduction of the contribution from all modes $k_y > k_y^{max}$. Numerical convergence has been ensured using a grid with $n_{k_x} \times n_{k_y} \times n_z \times n_{v_\parallel} \times n_\mu = 256 \times 48 \times 60 \times 48 \times 8$ and $k_{y,\min} = 0.03$ (further reduced to 0.025 for $a/L_{T_i} = 8$).

The recent work in Ref. [16] investigated the behavior of the zonal flows as a function of triangularity, concluding that the residual zonal flow decreases with decreasing triangularity (i.e.,

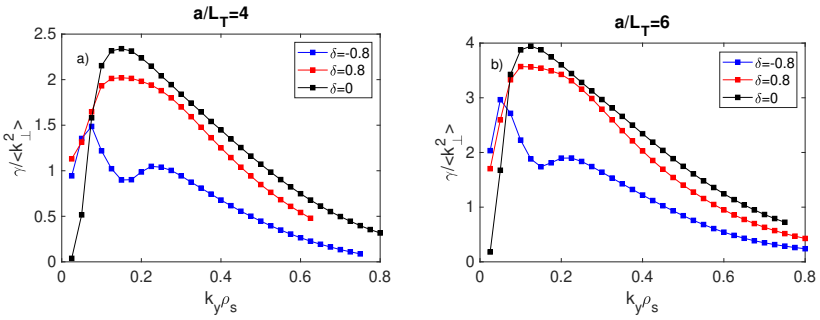

FIG. 10. Mixing length estimates computed accordingly to Eq. (14) for *a*) $a/L_T = 4$ and *b*) $a/L_T = 6$. Positive (negative) triangularity shown in red (blue); reference circular shape ($\delta = 0$) is shown in black.

is lower for negative triangularity than that for positive triangularity), and therefore suggests a weaker regulation of turbulence and transport by zonal flows when $\delta < 0$, claiming also that linear results are not able to explain the transport reduction. While this appears to be in contrast with our nonlinear results, we first connect our results to linear and quasilinear models. Since inverting the plasma shape alone is able to reduce the growth rates, the question of how much a quasilinear model is able to capture the effect of triangularity remains valid and we will show that one can extract useful information already from the linear behavior of the system.

To this end, in Figure 10 we plot the simplest mixing length estimate [24, 25] for the quasilinear weights w^{ql}

$$w^{\mathrm{ql}} = \frac{\gamma}{\langle k_\perp^2 \rangle}, \tag{14}$$

where $\langle k_\perp^2 \rangle$ is the flux-surface average of the squared perpendicular wave number weighted by the mode amplitude. These weights, describing the saturation levels of the nonlinear electrostatic potential, can be used to construct a quasilinear model [26] of the form

$$Q^{\mathrm{ql}} = A_0 \sum_{k_y} w^{\mathrm{ql}}_{k_y} Q^{\mathrm{l}}_{k_y}, \tag{15}$$

where A_0 is a scaling factor associated with the absolute fluctuation amplitude and $Q^{\mathrm{l}}_{k_y}$ is the linear spectral component to the flux associated to the k_y mode, i.e., the flux evaluated with the fields from the corresponding linear eigenmode. We refer to [26] and the references therein for the exact definition of Q^{l}. We see that the simple quasilinear estimate captures quite well the changes from

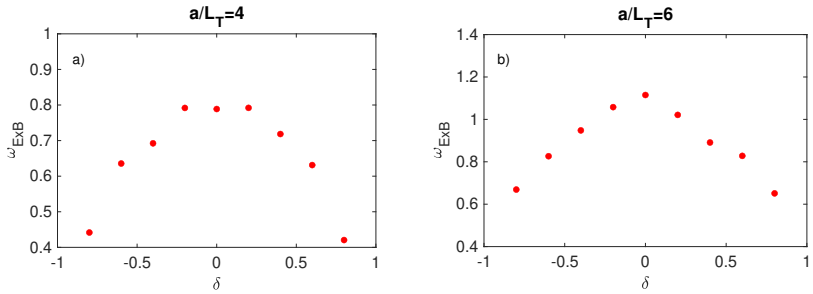

FIG. 11. Shearing rate $\omega_{\mathbf{E}\times\mathbf{B}}$ as a function of triangularity time averaged over the nonlinear saturated state for *a*) $a/L_T = 4$ and *b*) $a/L_T = 6$.

linear to nonlinear spectra, in particular the downshift in k_y as well as the presence of a double peak in the negative δ case. Simply using Eq. (14) is however unable to fully capture the dependence of the transport level on δ. In Figure 10 we also show the results obtained for a circular plasma ($\delta = 0$), which are very close to the ones obtained with positive triangularity and therefore indicate that assuming a shape independent scaling factor A_0 will not yield correct predictions. Building a quasilinear estimate that accounts for the effect of shape is possible but outside the scope of this paper. In particular such model should be based on a broader range of shaping parameters than the ones we have considered here. To investigate the origin of the discrepancy between quasilinear and nonlinear runs, we plot in Figure 11 the $\mathbf{E}\times\mathbf{B}$ shearing rate defined as

$$\omega_{\mathbf{E}\times\mathbf{B}} = \langle \frac{1}{B_0}\frac{\partial^2\phi}{\partial x^2}\rangle_t \tag{16}$$

where $\langle\cdot\rangle_t$ indicates a time average over the steady state of the simulation, to measure the impact of zonal flows on the saturation. We observe that increasing the magnitude of triangularity *lowers* the shearing rate, regardless of the sign of triangularity. This nonlinear effect must be accounted for explaining the impact of δ. Therefore, accounting also the results of Fig. 1, modifying the plasma shape adding $\delta < 0$ reduces at the same time linear growth rate and zonal flow shearing rate, such that the transport slightly increases. On the other hand, going from zero to positive triangularity, the growth rates increase and the shearing rates still diminish, thus resulting in a much more severe increase of transport with δ. Note that this is not in disagreement with Ref. [16] because if we consider the case at $a/L_T = 6$ (where the differences in transport are bigger), then

$\delta = -0.8$ roughly has the same transport level as $\delta = 0.4$ but the shearing rate is larger for the shape with $\delta > 0$.

A. Sensitivity to main plasma parameters

The results we have discussed in the previous section are clearly specific to the geometry we have considered, which is somewhat extreme. Such large values of triangularity are likely not achievable in a real tokamak, especially at mid-radius. Indeed, as already pointed out by Duff *et al.* [15], the aim of the simulations was not to investigate a specific experiment but rather to probe the effect of extreme values of triangularity on ITG. Nonetheless, even with this goal in mind it is fundamental to assess how much the result are robust with respect to reasonable variations of plasma parameters. We already observed a significant, larger than expected, effect of triangularity

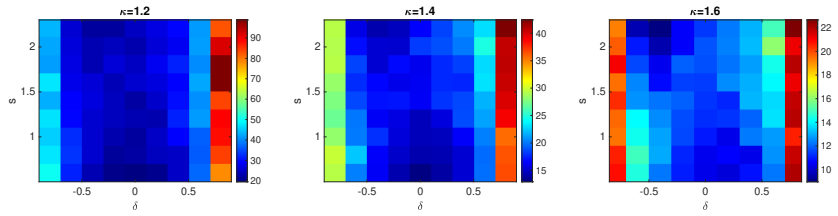

FIG. 12. Dependency on nonlinear hear fluxes on triangularity δ and magnetic shear s for different values of elongation κ. All simulations considered $q = 2$.

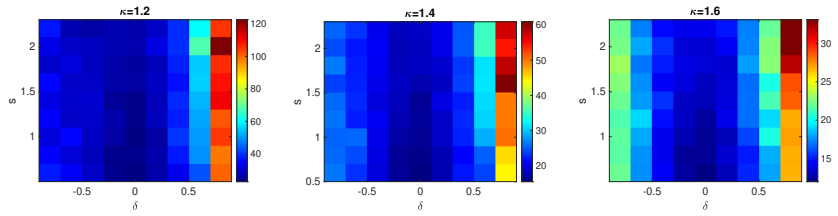

FIG. 13. Same as Figure 12 but showing results for $q = 4$.

shear (s_δ), therefore even if a proper sensitivity analysis is beyond the scope of this work, we have performed nonlinear simulations varying the main plasma parameters, considering in a first step

q, s, κ and δ (the robustness of the effect of s_δ will be addressed later) as shown in Figures 12 and 13. We point out that even if we are considering a very simplified physical model, the problem is already high dimensional and we cannot afford from a computational point of view to systematically vary all the relevant parameters including plasma gradients. Therefore, we performed this analysis only for $a/L_T = 6$ (difference between positive and negative δ appear more clearly) and focus solely on the effect of the magnetic geometry. Even with this simplification a brute force approach like the one we used is possible only thanks to the excellent performance of GENE on GPUs [27] (a single run can be performed on a single V100 GPU card of the Marconi100 Supercomputer) and for a more comprehensive parameter exploration more clever techniques, like the one discussed in Ref. [28], should be used. We have considered large variations for the mentioned parameters, with the exception of q for which we have only used two different values, $q = 2$ and $q = 4$. We observe that the dependence of fluxes with δ, that is the flux is larger for positive large δ compared to negative, remains. This difference diminishes if elongation is increased, with a strong overall reduction of transport when κ is large, in agreement with Ref. [29].

A somewhat surprising effect we observed is the strong role of the derivative of triangularity, captured by the parameter s_δ. Indeed, as clearly shown in Figure 8 going from the specific functional form in Eq. (4) to no radial variation of δ reduces the transport for positive triangularity to the point that we do not observe anymore any significant difference depending on the sign of δ but only a very weak dependence on $|\delta|$. Clearly, $s_\delta = 0$ is not a physically realistic choice since triangularity varies with radius and diminishes moving towards the magnetic axis, but this result points out how the radial variation of shaping coefficients is a key ingredient in setting the overall transport level. Similar observations have already been made regarding the effect of elongation on turbulent transport, see [30]. We have probed the sensitivity to δ and s_δ by performing a dedicated nonlinear scan for both values of temperature gradient as shown in Figures 14 and 15. We observe that for both gradients, positive triangularity is significantly more affected by variation of s_δ with the transport strongly increasing as s_δ becomes large. This observation is particularly relevant because it implies that even if negative triangularity rapidly diminishes with radius it can still lead to a strong suppression of fluxes over a narrow region with respect to its positive counterpart. This in turn suggests that confinement improvement can also be expected for large devices. In this case even if ρ^* (the ratio between the Larmor radius and the machine minor radius usually used to describe the magnitude of nonlocal effects) is small, the rapid variation of δ with radius near the plasma edge may result in a significant turbulence suppression, effectively acting as a transport

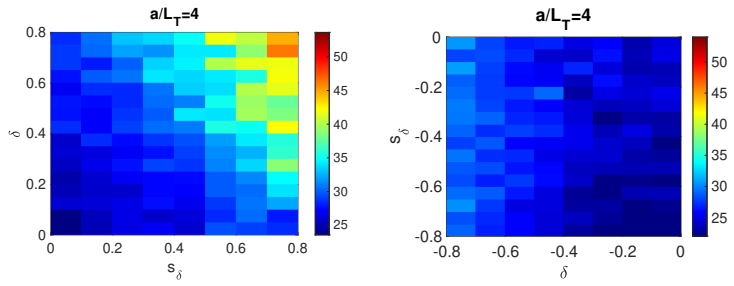

FIG. 14. Sensitivity of the fluxes to δ and s_δ, on the left for positive triangularity and on the right for negative.

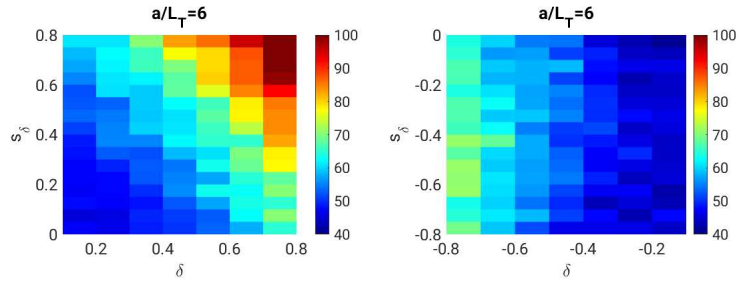

FIG. 15. Same as Figure 14 but showing results for $a/L_T = 6$.

barrier. This possibility shall be further investigated by considering more realistic geometries and plasma profiles, either obtained from actual experiments or from integrated modeling, as well as by adopting a higher fidelity model, i.e. a kinetic electron response. We leave this for future work.

VI. SUMMARY AND OUTLOOK

Considering the case discussed in Ref. [15], we have revisited the impact of (large) positive and negative triangularity on electrostatic ITG turbulence modelled with adiabatic electrons. The bulk of the simulations presented have been performed using the flux-tube version of the GENE code; to strengthen the results the key findings have also been validated with dedicated GKW runs obtaining excellent agreement. Point-by-point conclusions follow.

- Differently from what previously reported, we find that triangularity does influence transport, with larger fluxes when δ is flipped from negative to positive. Negative triangularity *lowers* the linear growth rates such that simple quasilinear estimates already predict a transport reduction with respect to its mirror shape.

- The actual transport level is nonetheless crucially set by the zonal flows, which are affected by the plasma shape. The zonal flow shearing rate is reduced as triangularity is increased in magnitude regardless of its sign, but the lower growth rates associated with $\delta < 0$ allow the transport to be lower when δ is negative. We have verified the robustness of these results by performing extensive nonlinear scans over the main plasma shape parameters.

- We find that a crucial parameter setting the transport level is the derivative of triangularity, s_δ. The observed difference between positive and negative triangularity disappears if s_δ is made smaller. Although we have used a model geometry, this results is particularly relevant because it implies that even if triangularity is rapidly diminishing, it can still strongly reduce the transport over the narrow region where it stays finite. This suggests that confinement improvement can also be expected for larger devices where the always present reduction of δ with radius could itself lead to a transport reduction, even without nonlocal effects.

The analysis that has been presented in this work could be extended in different ways. First, given the clear importance of the details of the geometry including the radial derivatives of the shaping coefficients, the impact of exotic plasma shapes should be explored in a systematic way considering a more complete set of shapes, as for example the ones discussed in Ref. [31]. While such an investigation is computationally very expensive, it is currently possible thanks to both the excellent code performance on GPUs as well as the availability of advanced techniques for sensitivity analysis [28]. The results of such an analysis could then be used to identify particularly promising plasma shapes and optimise them in conjunction with other relevant plasma parameters, such as magnetic shear [13]. This study should then be extended to include kinetic electrons and explore other turbulent regimes. Finally, the overall impact of shaping must be addressed in the context of profile prediction. It is essential to account for the global nature of a plasma equilibrium in order to properly assess whether the (potentially radially localized as the effect stemming from s_δ) transport reduction observed here translates into an overall confinement improvement or not.

ACKNOWLEDGMENTS

G.M. gladly acknowledges stimulating discussion with A. Marinoni and D. Told which motivated this work. We acknowledge the EuroHPC Joint Undertaking for awarding this project access to the EuroHPC supercomputer LUMI, hosted by CSC (Finland) and the LUMI consortium through a EuroHPC Regular Access call. Part of the simulations were performed on the M100 supercomuper at CINECA. This work was partly supported by the Exascale Computing Project (17-SC-20-SC), a collaborative effort of the U.S. Department of Energy Office of Science and the National Nuclear Security Administration.

[1] F. Wagner, G. Becker, K. Behringer, D. Campbell, A. Eberhagen, W. Engelhardt, G. Fussmann, O. Gehre, J. Gernhardt, G. v. Gierke, G. Haas, M. Huang, F. Karger, M. Keilhacker, O. Klüber, M. Kornherr, K. Lackner, G. Lisitano, G. G. Lister, H. M. Mayer, D. Meisel, E. R. Müller, H. Murmann, H. Niedermeyer, W. Poschenrieder, H. Rapp, H. Röhr, F. Schneider, G. Siller, E. Speth, A. Stäbler, K. H. Steuer, G. Venus, O. Vollmer, and Z. Yü, Phys. Rev. Lett. **49**, 1408 (1982).

[2] A. Pochelon, T. Goodman, M. Henderson, C. Angioni, R. Behn, S. Coda, F. Hofmann, J.-P. Hogge, N. Kirneva, A. Martynov, J.-M. Moret, Z. Pietrzyk, F. Porcelli, H. Reimerdes, J. Rommers, E. Rossi, O. Sauter, M. Tran, H. Weisen, S. Alberti, S. Barry, P. Blanchard, P. Bosshard, R. Chavan, B. Duval, Y. Esipchuck, D. Fasel, A. Favre, S. Franke, I. Furno, P. Gorgerat, P.-F. Isoz, B. Joye, J. Lister, X. Llobet, J.-C. Magnin, P. Mandrin, A. Manini, B. Marlétaz, P. Marmillod, Y. Martin, J.-M. Mayor, J. Mlynar, C. Nieswand, P. Paris, A. Perez, R. Pitts, K. Razumova, A. Refke, E. Scavino, A. Sushkov, G. Tonetti, F. Troyon, W. V. Toledo, and P. Vyas, Nuclear Fusion **39**, 1807 (1999).

[3] M. E. Austin, A. Marinoni, M. L. Walker, M. W. Brookman, J. S. deGrassie, A. W. Hyatt, G. R. McKee, C. C. Petty, T. L. Rhodes, S. P. Smith, C. Sung, K. E. Thome, and A. D. Turnbull, Phys. Rev. Lett. **122**, 115001 (2019).

[4] A. Marinoni, O. Sauter, and S. Coda, Reviews of Modern Plasma Physics **5** (2021), https://doi.org/10.1007/s41614-021-00054-0.

[5] E. A. Belli, G. W. Hammett, and W. Dorland, Physics of Plasmas **15**, 092303 (2008), https://pubs.aip.org/aip/pop/article-pdf/doi/10.1063/1.2972160/15873912/092303_1_online.pdf.

[6] A. Marinoni, S. Brunner, Y. Camenen, S. Coda, J. P. Graves, X. Lapillonne, A. Pochelon, O. Sauter, and L. Villard, Plasma Physics and Controlled Fusion **51**, 055016 (2009).

[7] G. Merlo, S. Brunner, O. Sauter, Y. Camenen, T. Görler, F. Jenko, A. Marinoni, D. Told, and L. Villard, Plasma Physics and Controlled Fusion **57**, 054010 (2015).

[8] G. Merlo, M. Fontana, S. Coda, D. Hatch, S. Janhunen, L. Porte, and F. Jenko, Physics of Plasmas **26**, 102302 (2019).

[9] R. Davies, D. Dickinson, and H. Wilson, Plasma Physics and Controlled Fusion **64**, 105001 (2022).

[10] G. D. Giannatale, P. Donnel, L. Villard, A. Bottino, S. Brunner, E. Lanti, B. F. McMillan, A. Mishchenko, M. Murugappan, and T. Hayward-Schneider, Journal of Physics: Conference Series **2397**, 012002 (2022).

[11] J. Ball and S. Brunner, Plasma Physics and Controlled Fusion **65**, 014004 (2022).

[12] R. Gaur, I. G. Abel, D. Dickinson, and W. D. Dorland, Journal of Plasma Physics **89**, 905890112 (2023).

[13] G. Merlo and F. Jenko, Journal of Plasma Physics **89**, 905890104 (2023).

[14] E. G. Highcock, N. R. Mandell, M. Barnes, and W. Dorland, Journal of Plasma Physics **84**, 905840208 (2018).

[15] J. M. Duff, B. J. Faber, C. C. Hegna, M. J. Pueschel, and P. W. Terry, Physics of Plasmas **29**, 012303 (2022).

[16] R. Singh and P. Diamond, Nuclear Fusion **62**, 126073 (2022).

[17] F. Jenko, W. Dorland, M. Kotschenreuther, and B. N. Rogers, Physics of Plasmas **7** (2000).

[18] A. J. Brizard and T. S. Hahm, Rev. Mod. Phys. **79**, 421 (2007).

[19] J. Candy, Plasma Physics and Controlled Fusion **51**, 105009 (2009).

[20] A. Peeters, Y. Camenen, F. Casson, W. Hornsby, A. Snodin, D. Strintzi, and G. Szepesi, Computer Physics Communications **180**, 2650 (2009), 40 YEARS OF CPC: A celebratory issue focused on quality software for high performance, grid and novel computing architectures.

[21] G. Merlo, O. Sauter, S. Brunner, A. Burckel, Y. Camenen, F. J. Casson, W. Dorland, E. Fable, T. Görler, F. Jenko, A. G. Peeters, D. Told, and L. Villard, Physics of Plasmas **23** (2016).

[22] T. Görler, X. Lapillonne, S. Brunner, T. Dannert, F. Jenko, F. Merz, and D. Told, Journal of Computational Physics **230**, 7053 (2011).

[23] J. Duff, Private communication.

[24] T. Dannert and F. Jenko, Physics of Plasmas **12**, 072309 (2005).

[25] F. Jenko, T. Dannert, and C. Angioni, Plasma Physics and Controlled Fusion **47**, B195 (2005).

[26] A. Mariani, S. Brunner, J. Dominski, A. Merle, G. Merlo, O. Sauter, T. Görler, F. Jenko, and D. Told, Physics of Plasmas **25**, 012313 (2018).

[27] K. Germaschewski, B. Allen, T. Dannert, M. Hrywniak, J. Donaghy, G. Merlo, S. Ethier, E. D'Azevedo, F. Jenko, and A. Bhattacharjee, Physics of Plasmas **28**, 062501 (2021).

[28] I. Farcas, G. Merlo, and F. Jenko, Communications Engineering **1** (2022).

[29] P. Angelino, X. Garbet, L. Villard, A. Bottino, S. Jolliet, P. Ghendrih, V. Grandgirard, B. F. McMillan, Y. Sarazin, G. Dif-Pradalier, and T. M. Tran, Phys. Rev. Lett. **102**, 195002 (2009).

[30] J. E. Kinsey, R. E. Waltz, and J. Candy, Physics of Plasmas **14**, 102306 (2007).

[31] R. Arbon, J. Candy, and E. A. Belli, Plasma Physics and Controlled Fusion **63**, 012001 (2021).

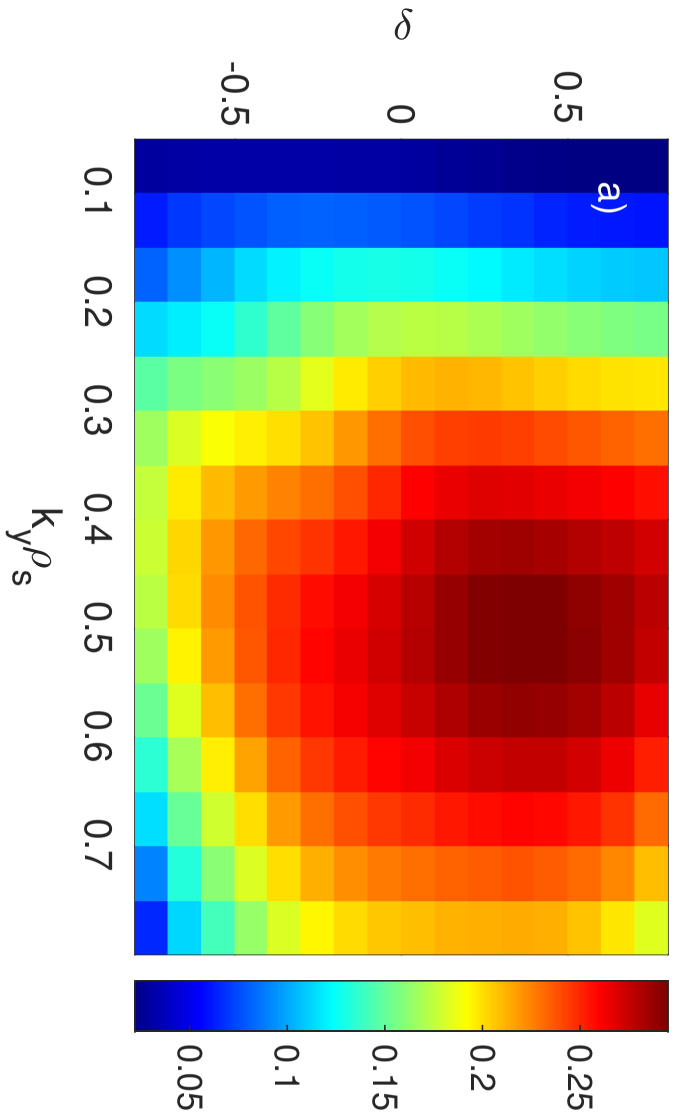

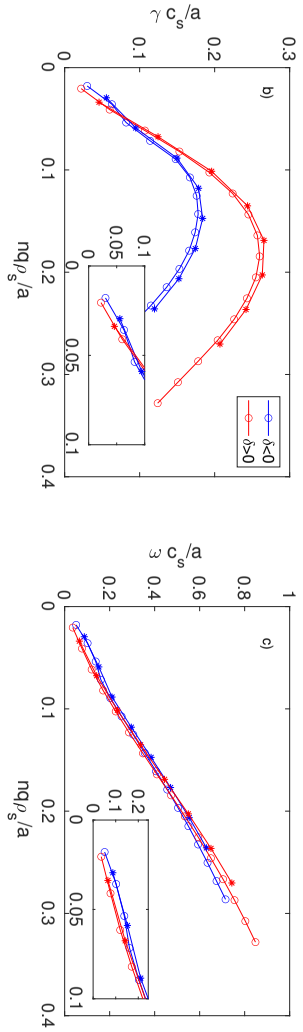

PLEASE CITE THIS ARTICLE AS DOI: 10.1063/5.0167292

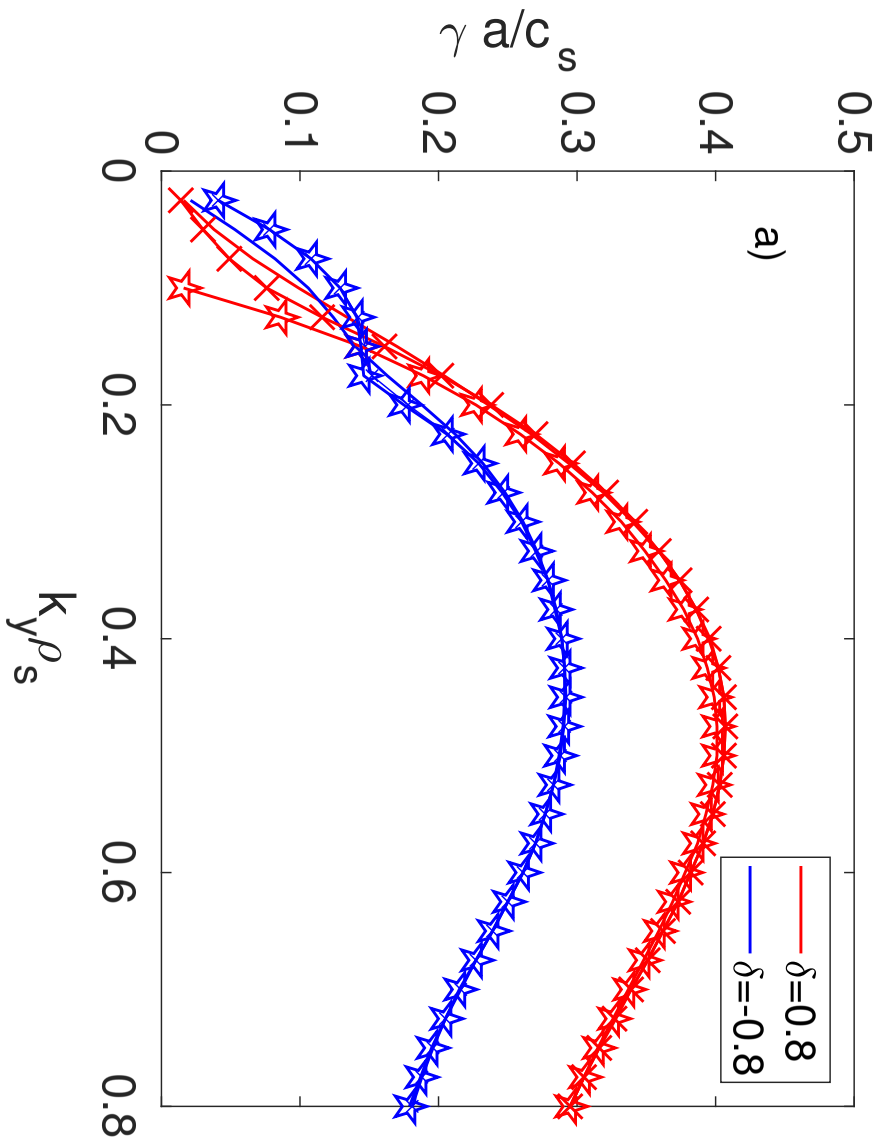

PLEASE CITE THIS ARTICLE AS DOI: 10.1063/5.0167292

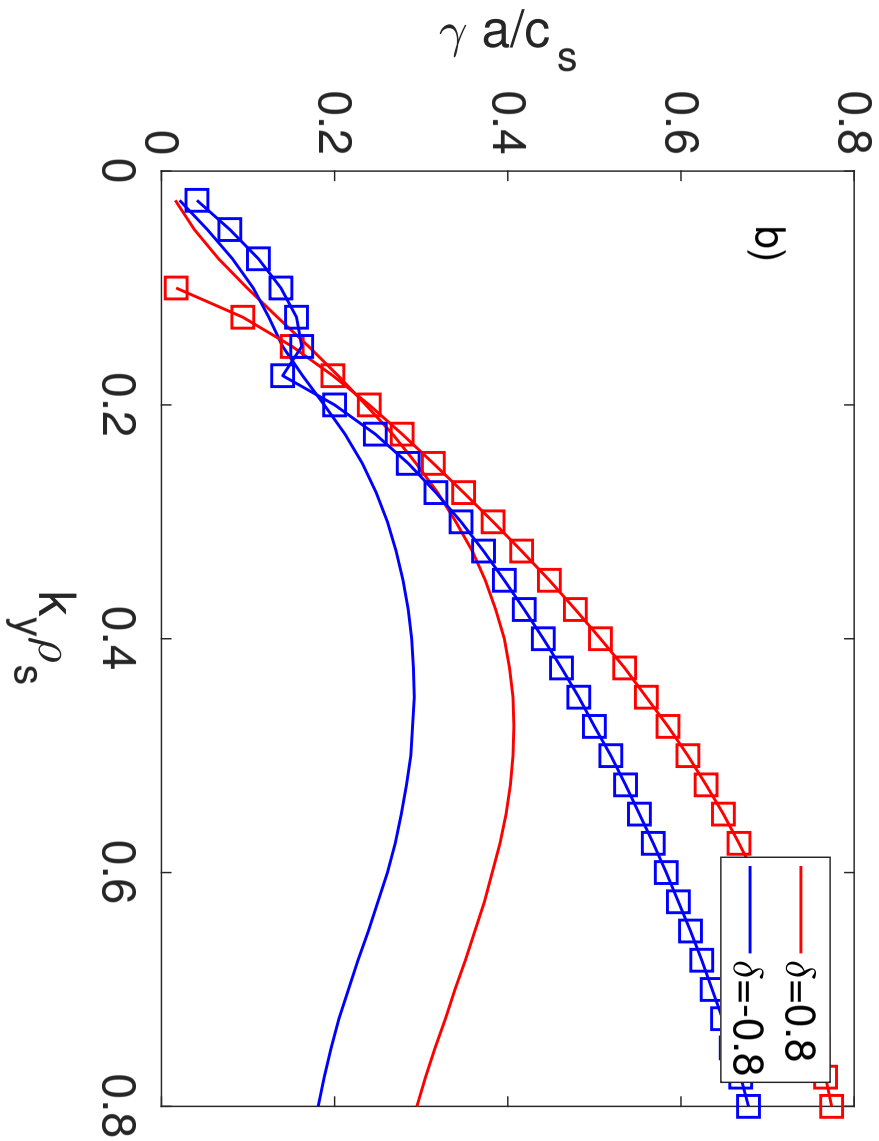

Physics of Plasmas

PLEASE CITE THIS ARTICLE AS DOI: 10.1063/5.0167292

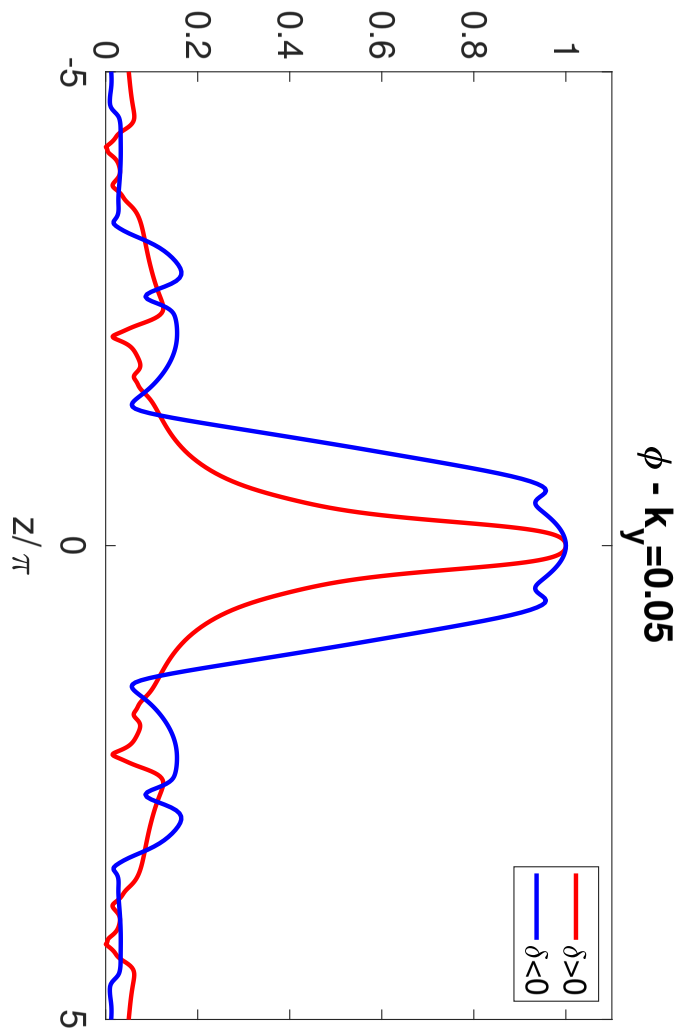

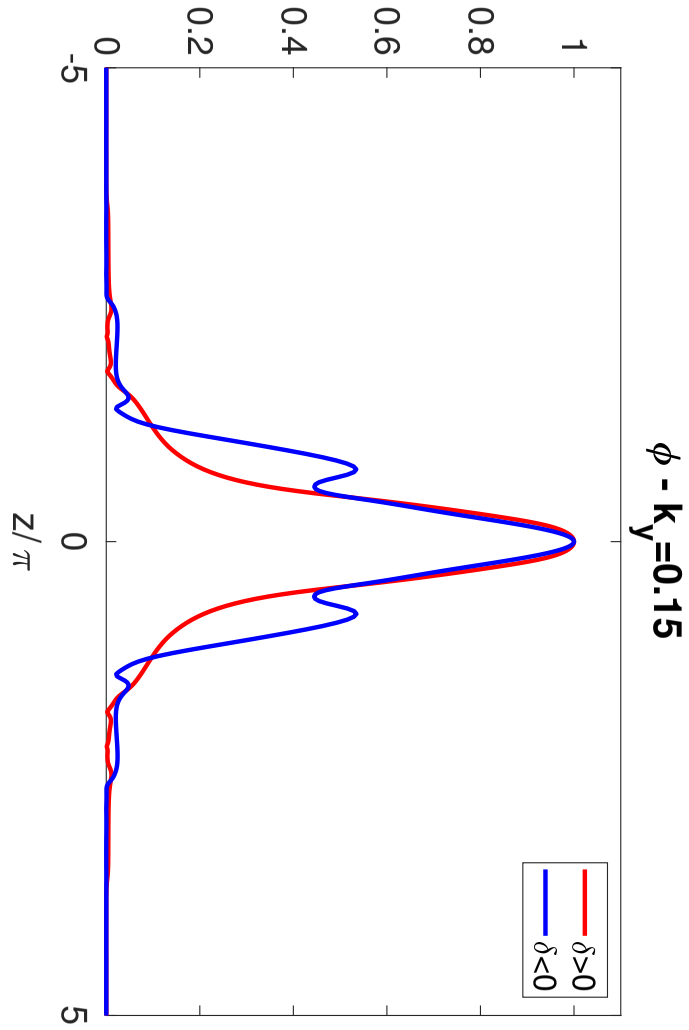

Physics of Plasmas

PLEASE CITE THIS ARTICLE AS DOI: 10.1063/5.0167292

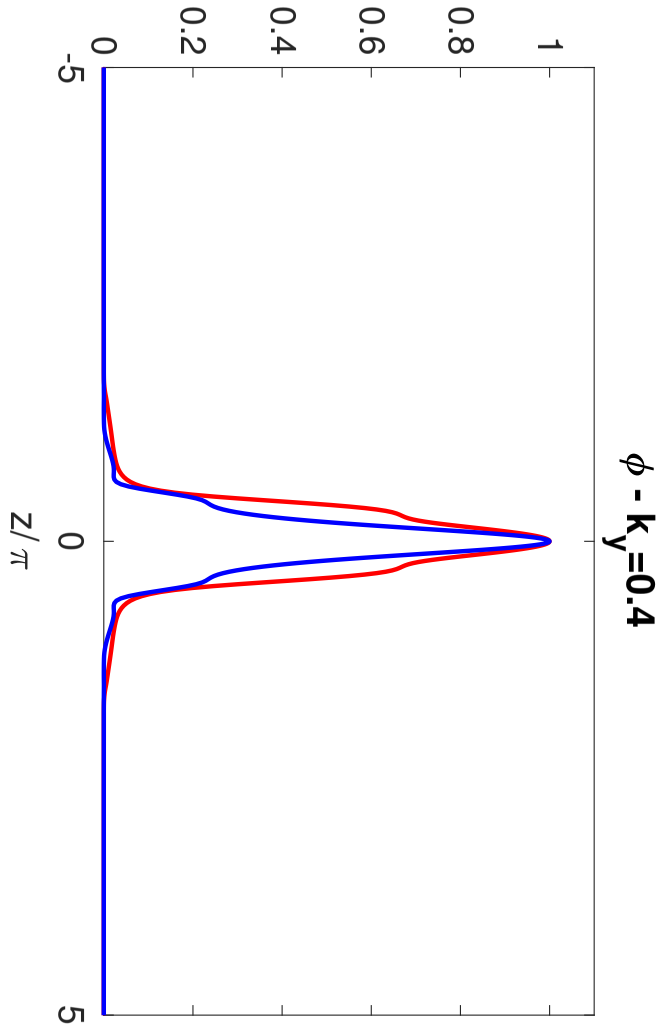

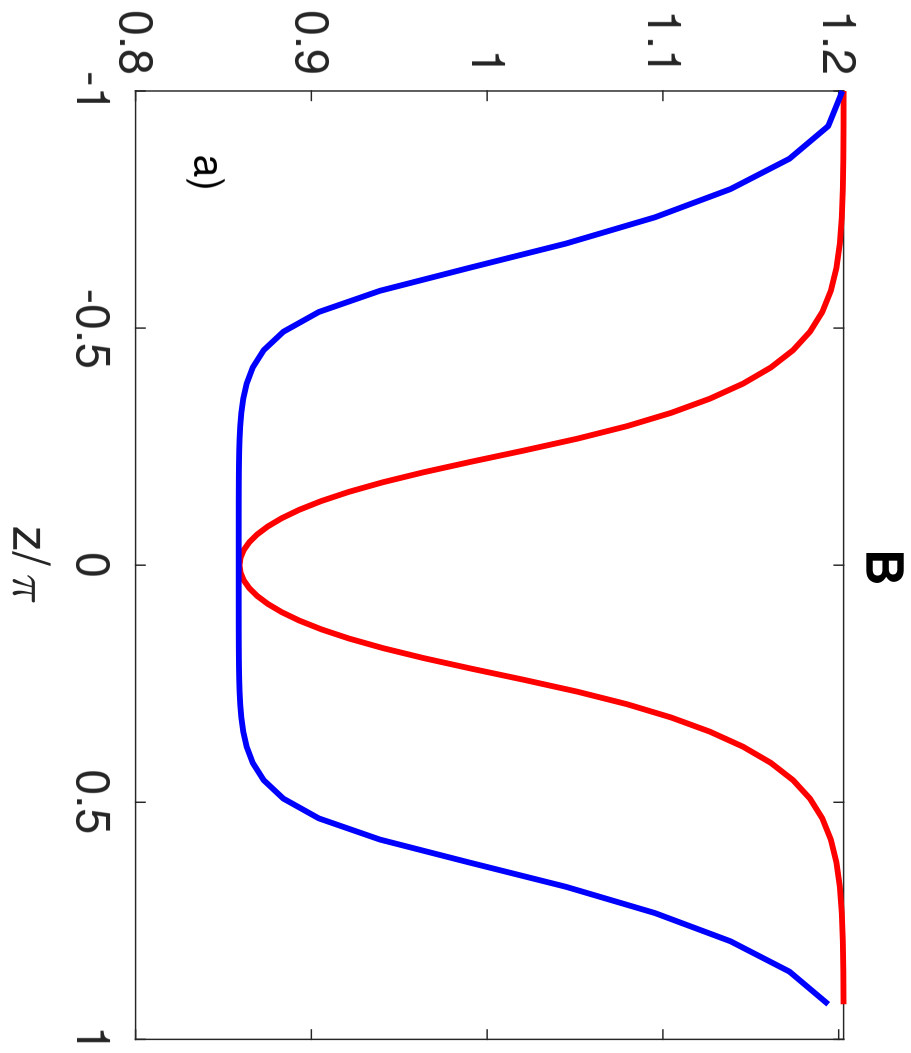

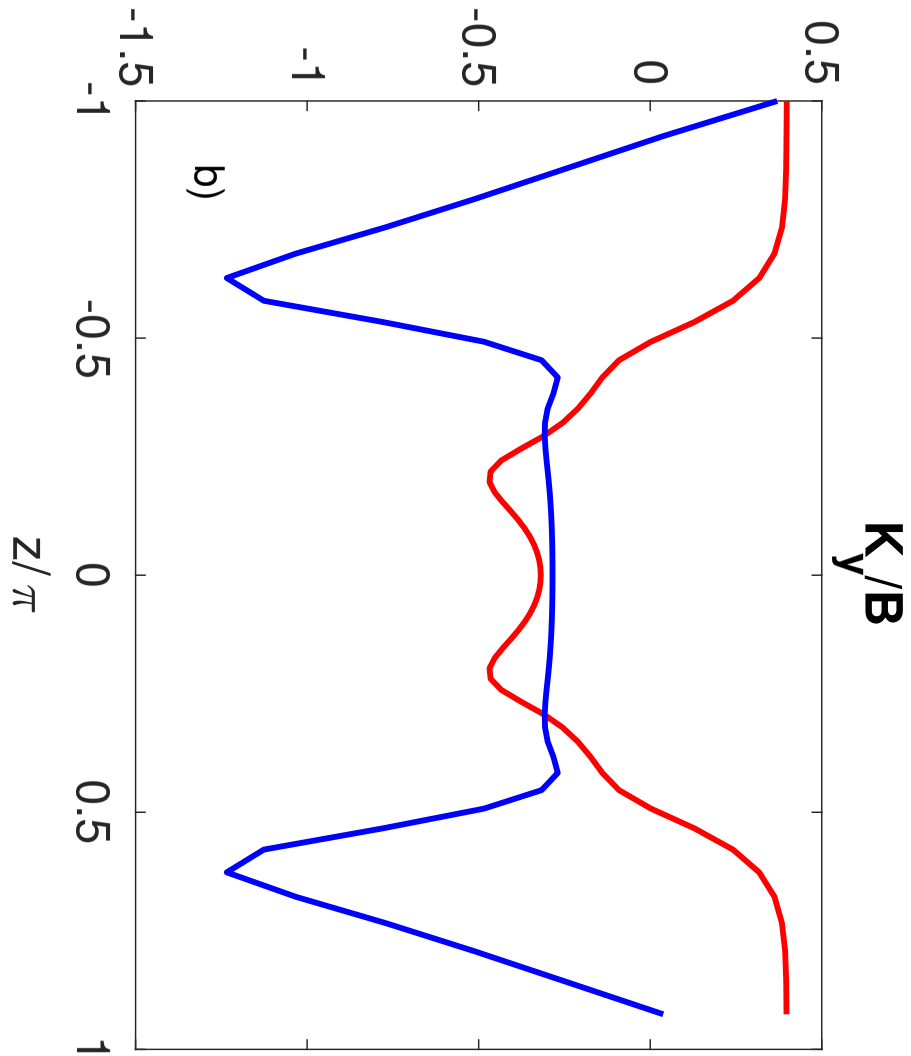

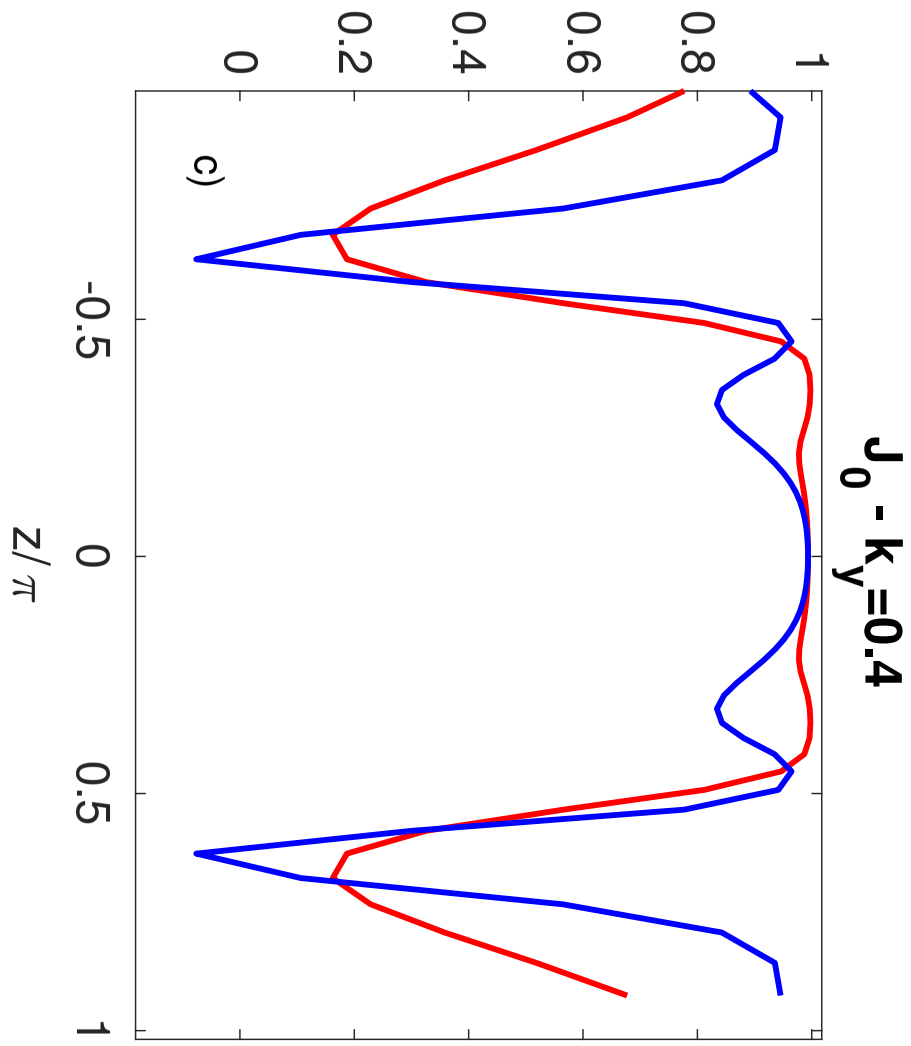

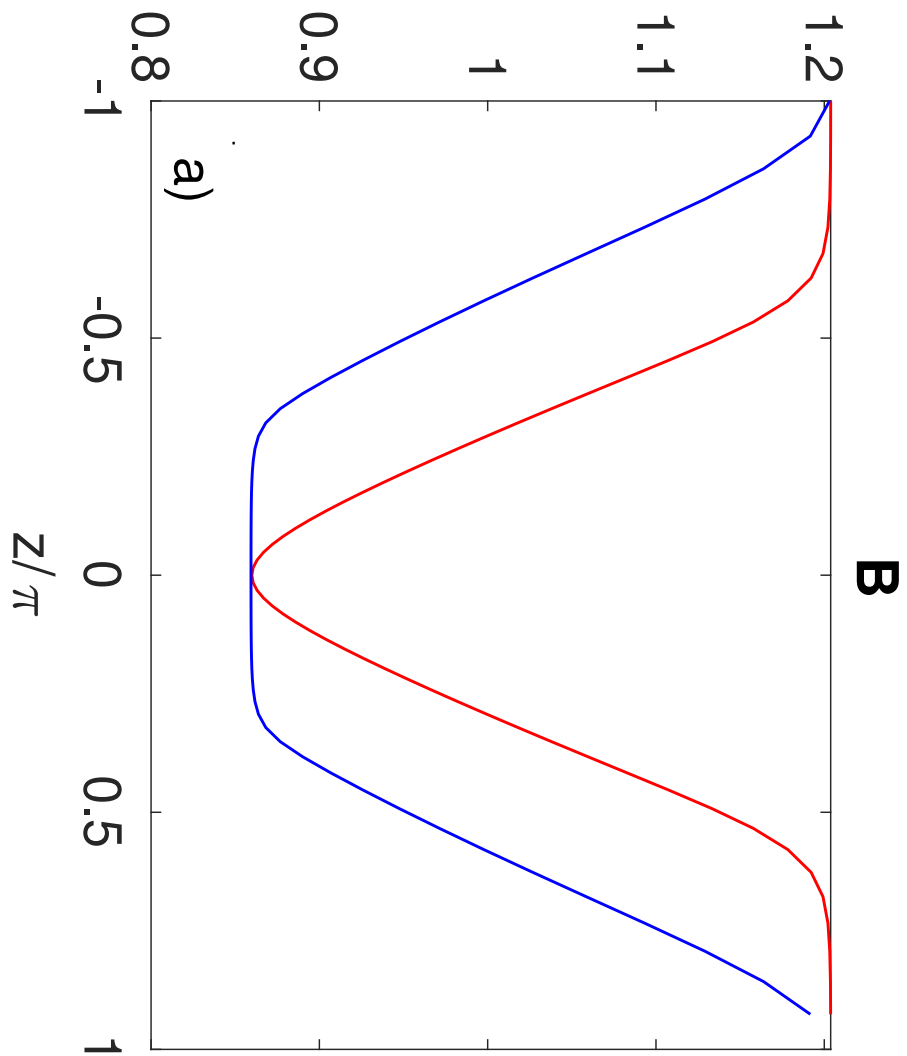

PLEASE CITE THIS ARTICLE AS DOI: 10.1063/5.0167292

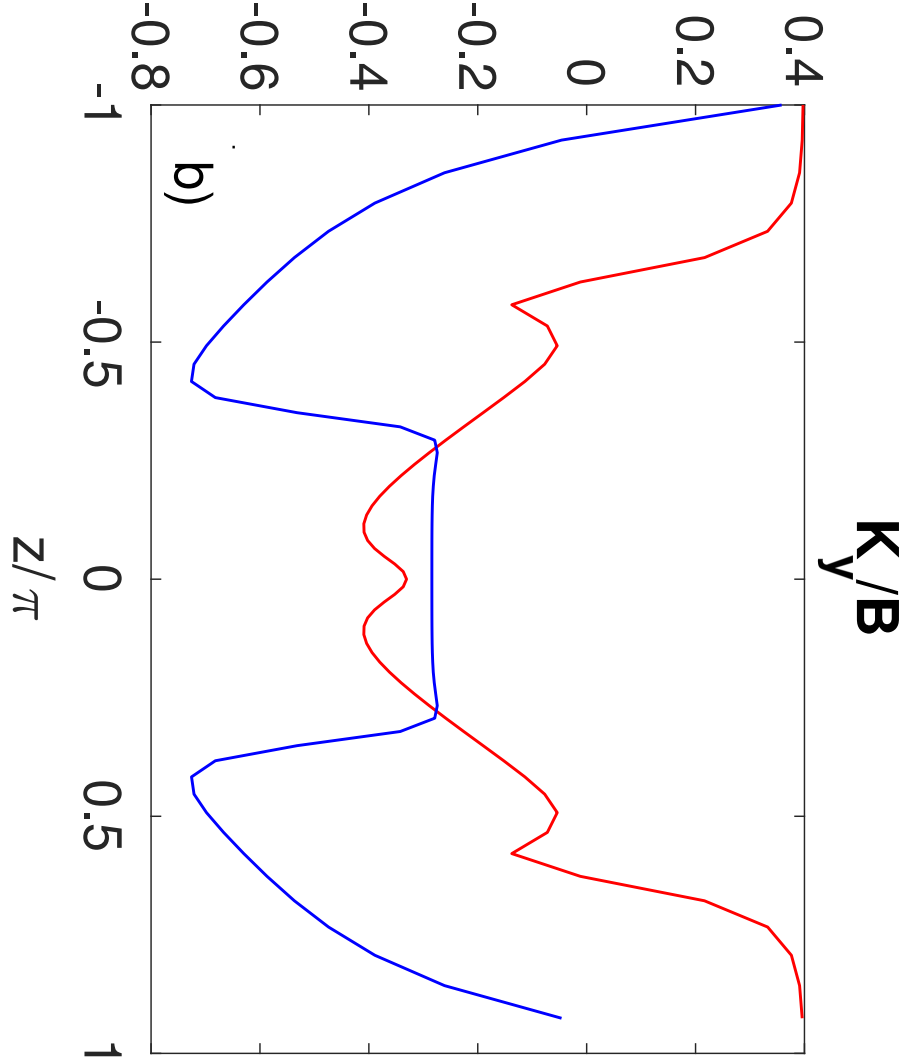

PLEASE CITE THIS ARTICLE AS DOI: 10.1063/5.0167292

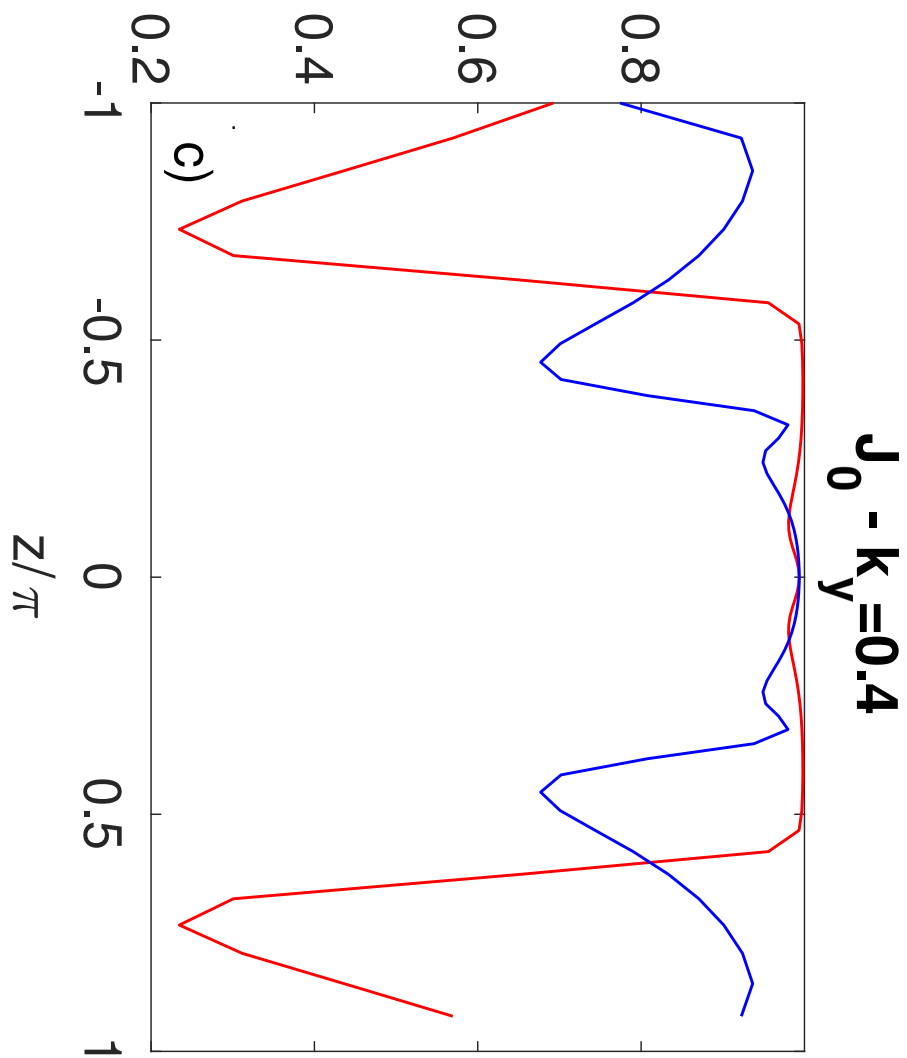

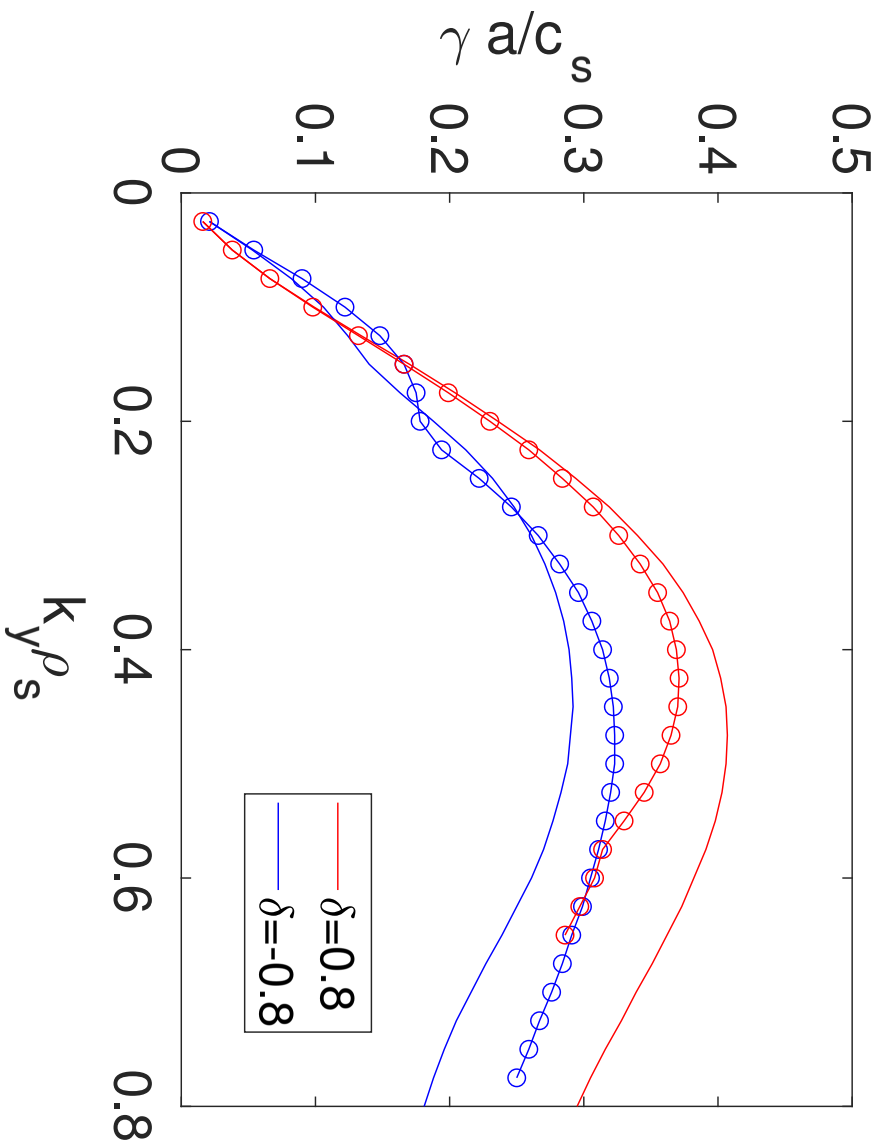

PLEASE CITE THIS ARTICLE AS DOI: 10.1063/5.0167292

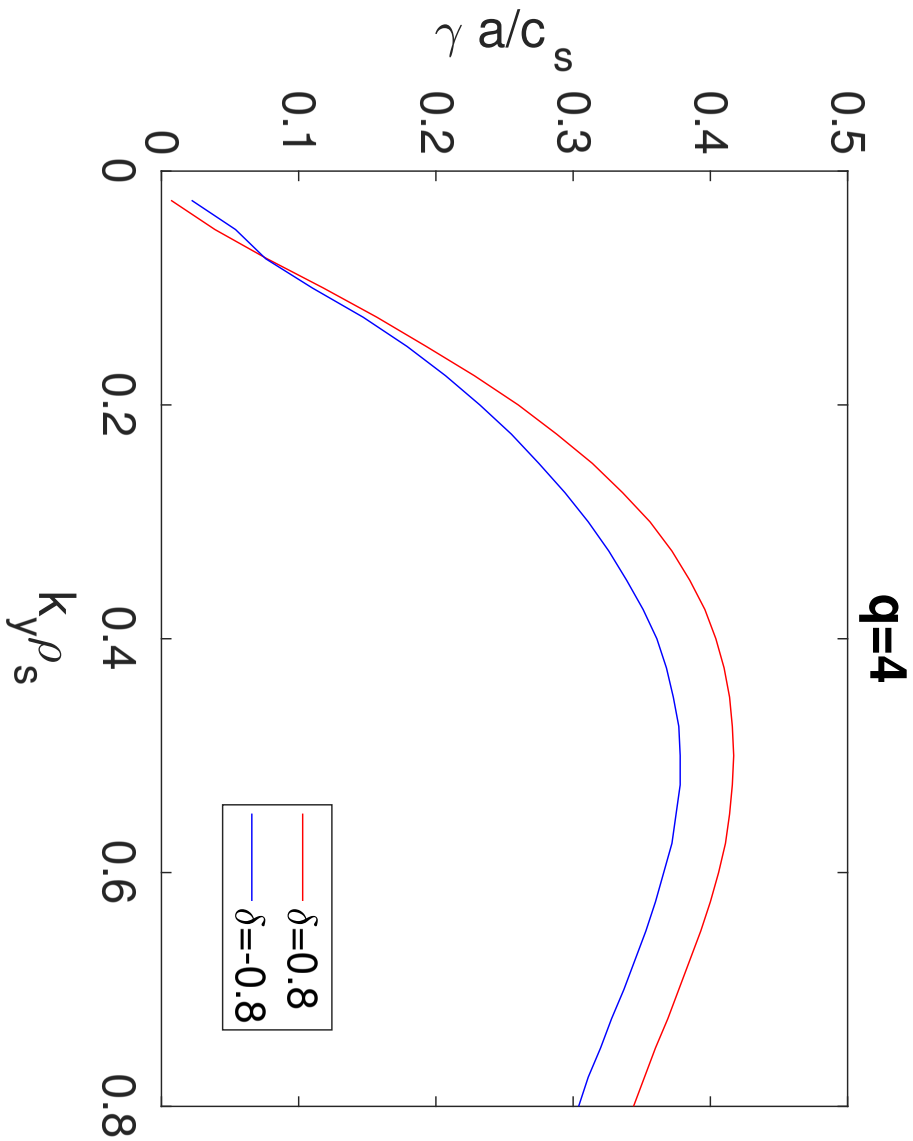

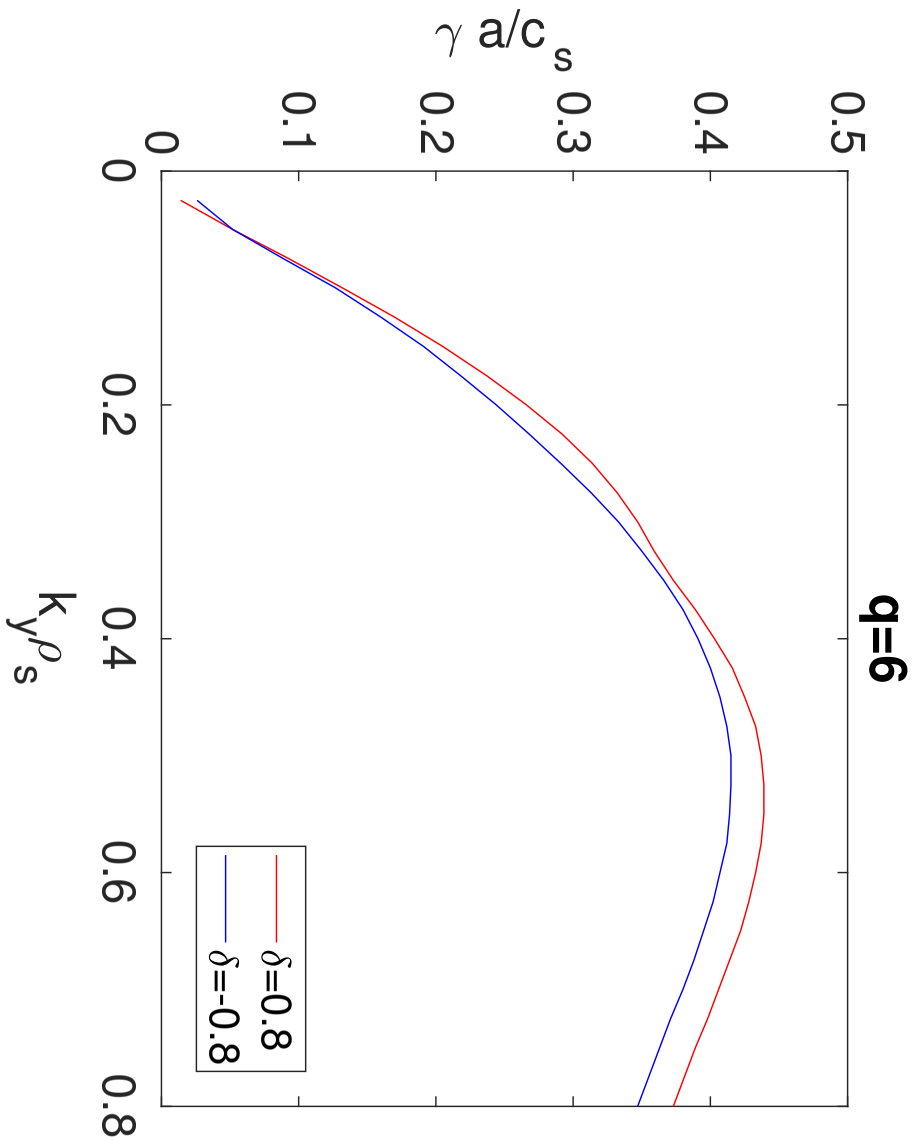

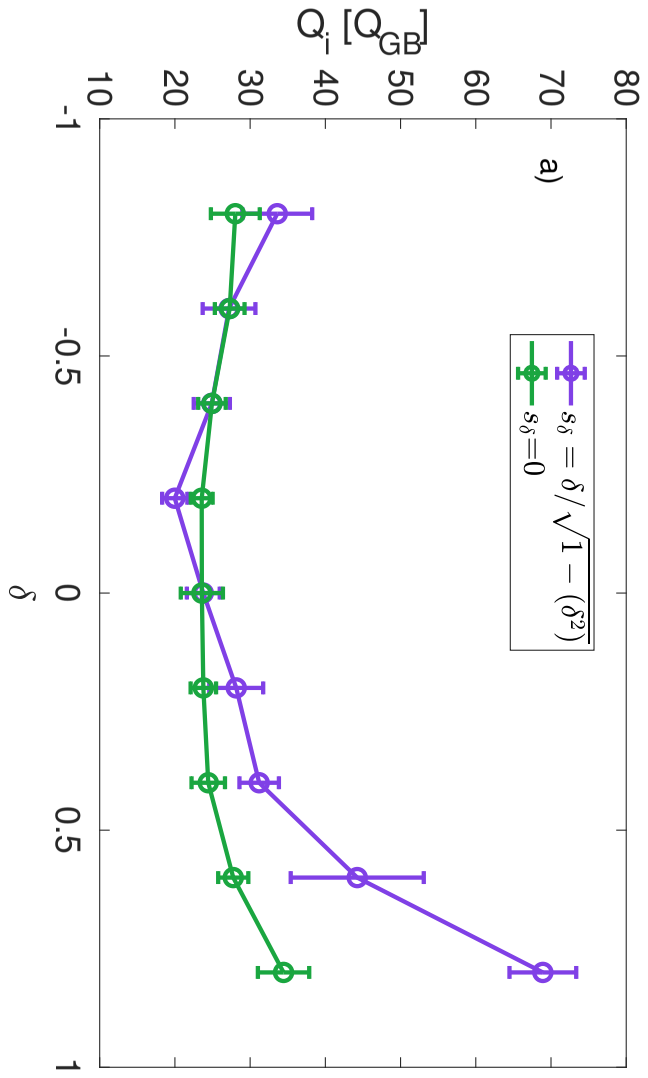

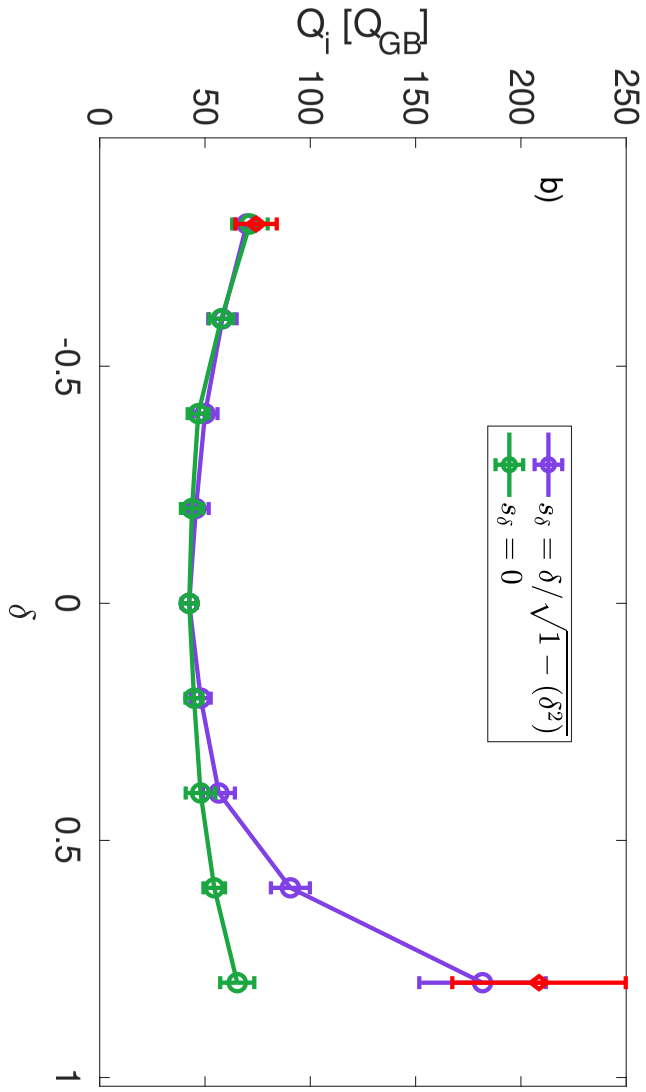

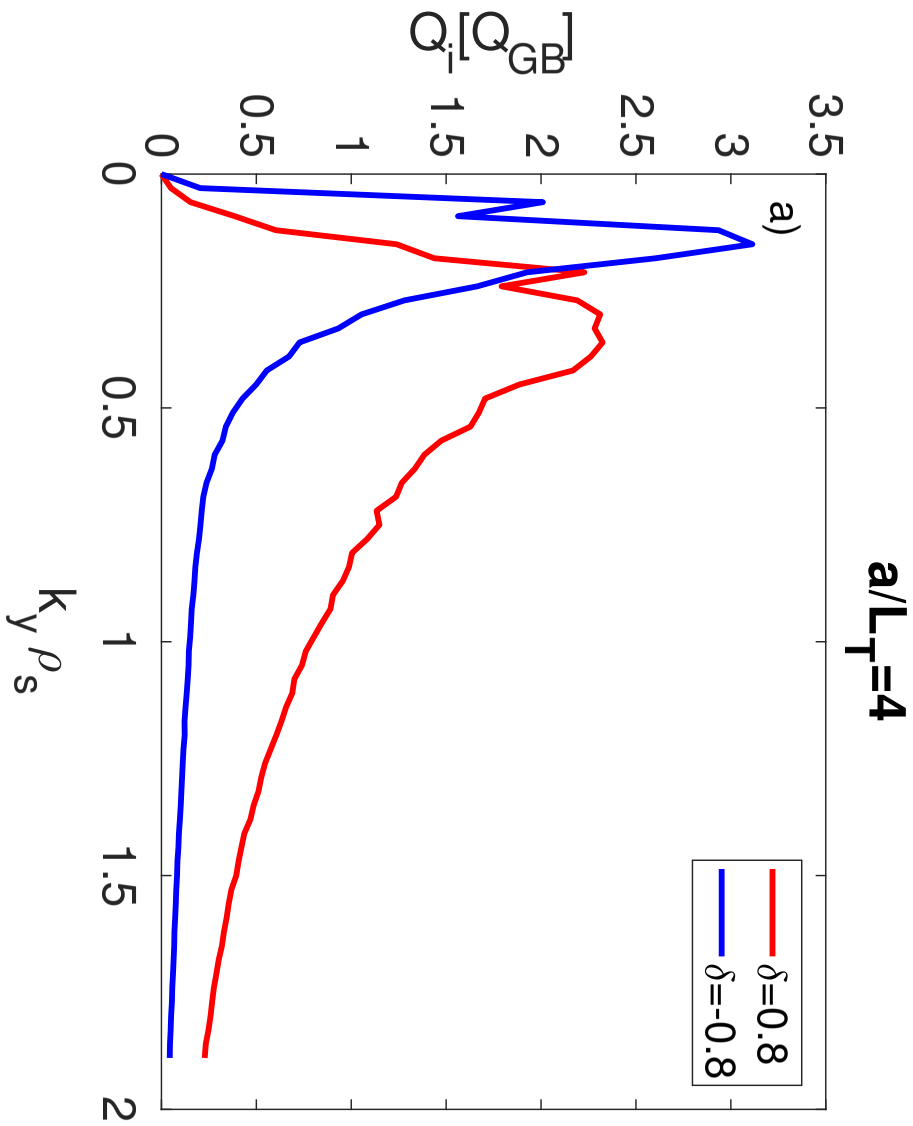

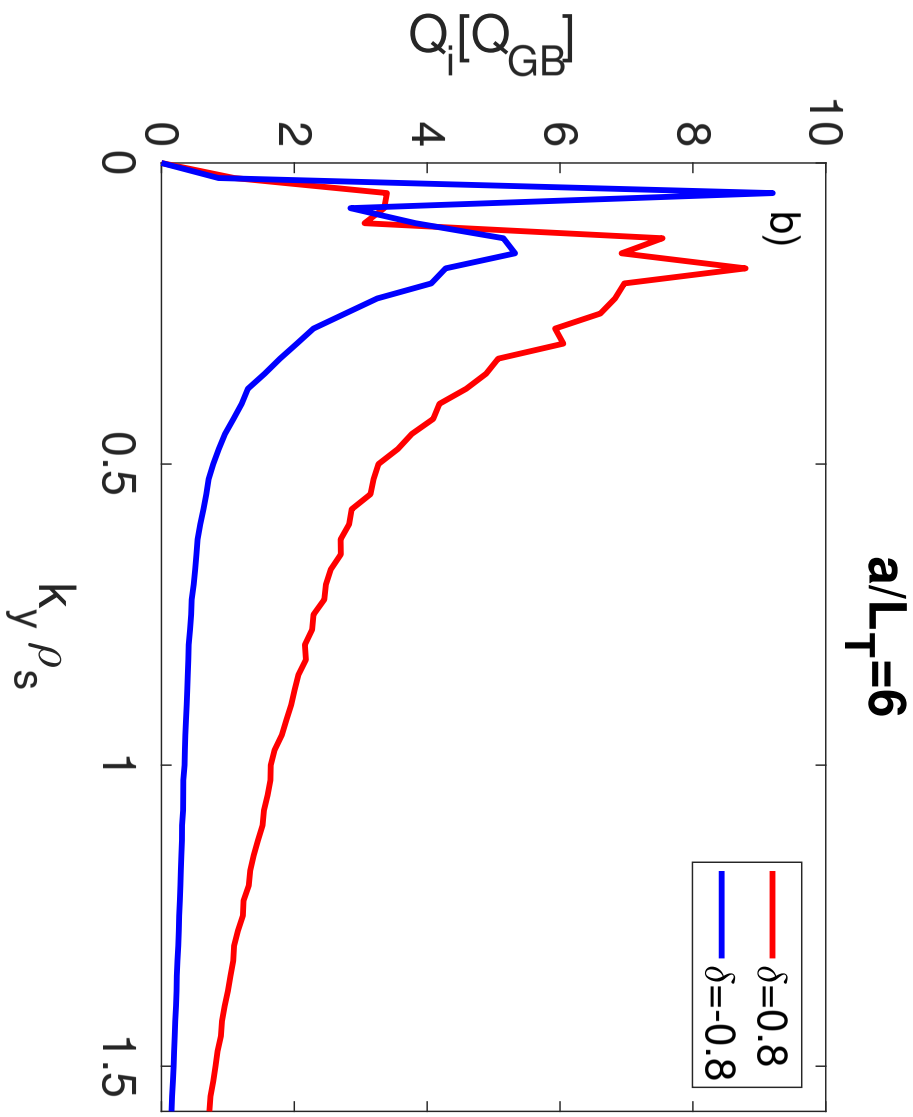

Physics of Plasmas

PLEASE CITE THIS ARTICLE AS DOI: 10.1063/5.0167292

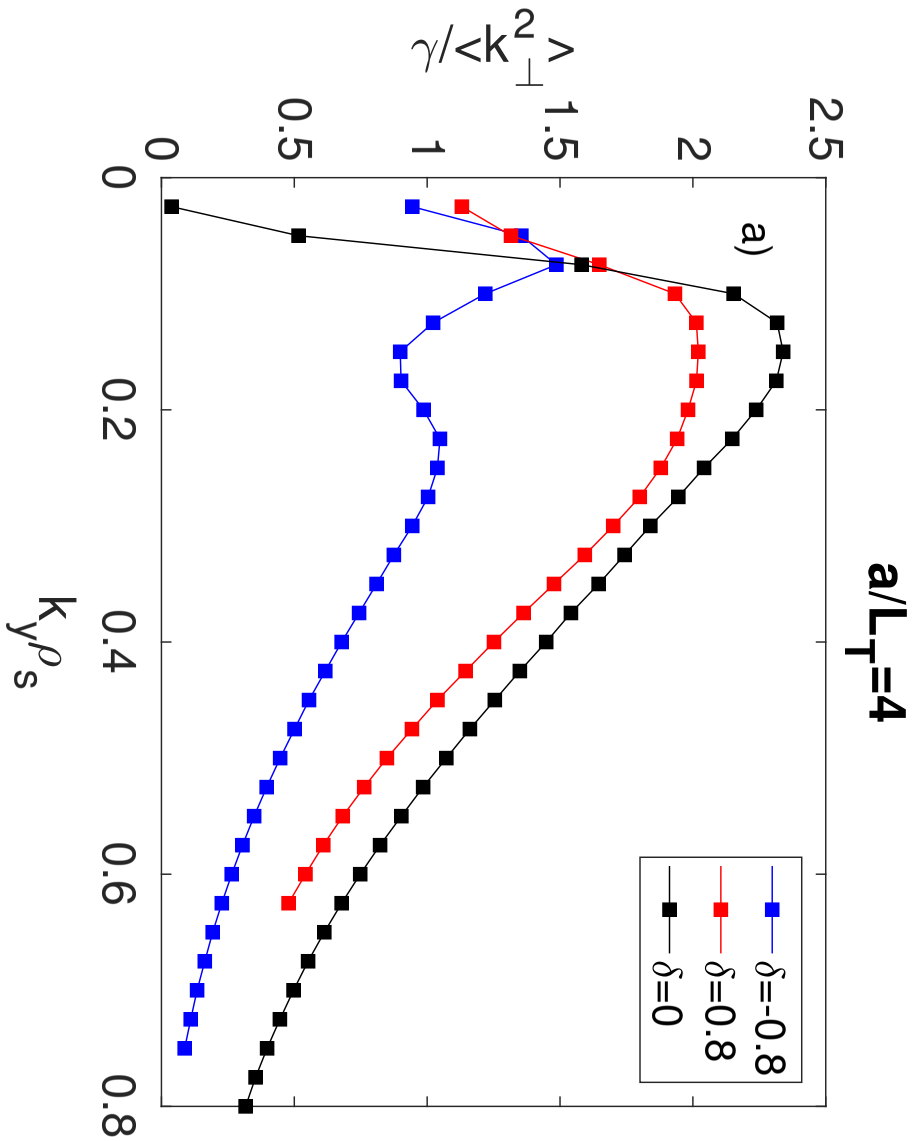

PLEASE CITE THIS ARTICLE AS DOI: 10.1063/5.0167292

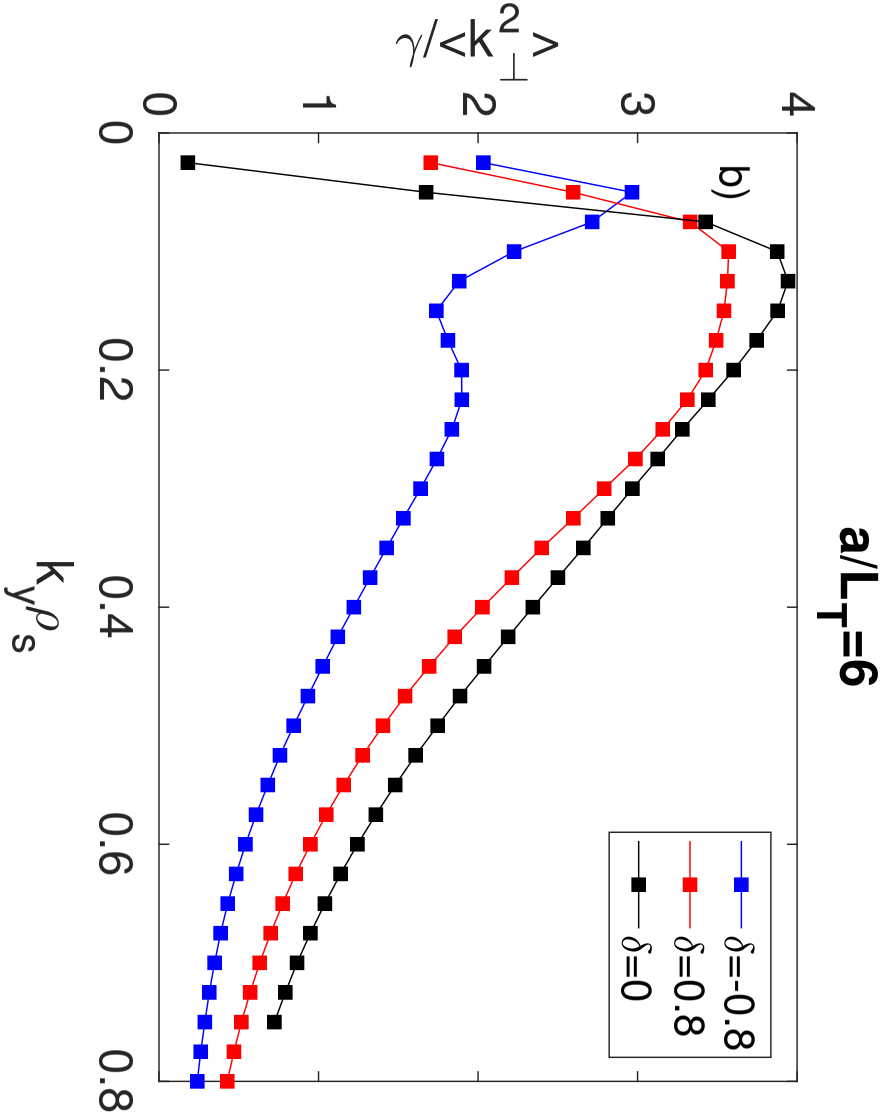

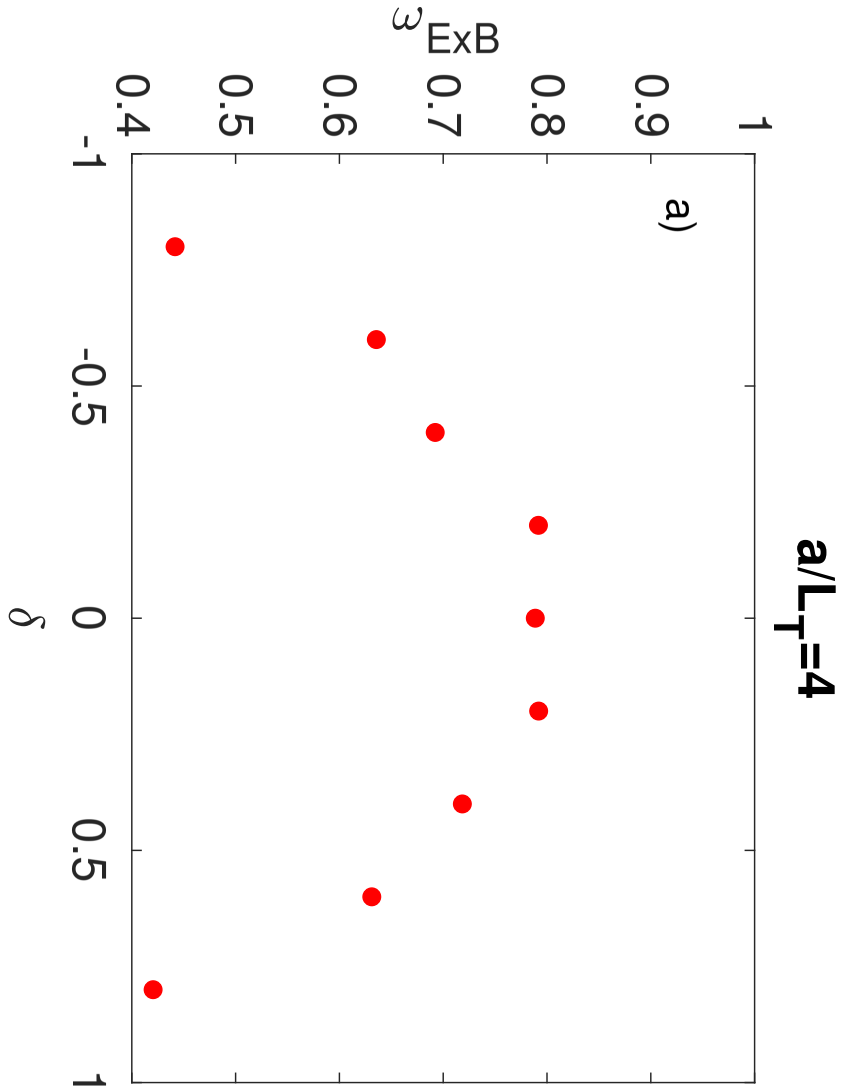

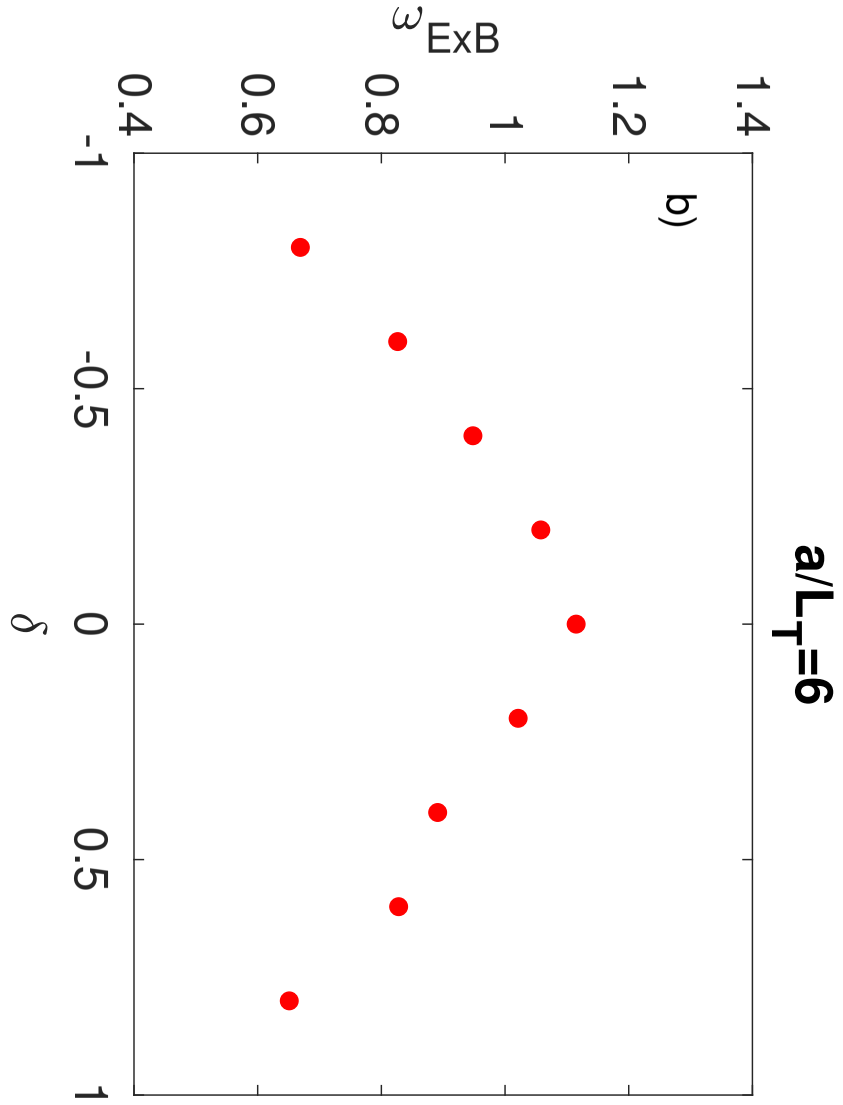

Physics of Plasmas

PLEASE CITE THIS ARTICLE AS DOI: 10.1063/5.0167292

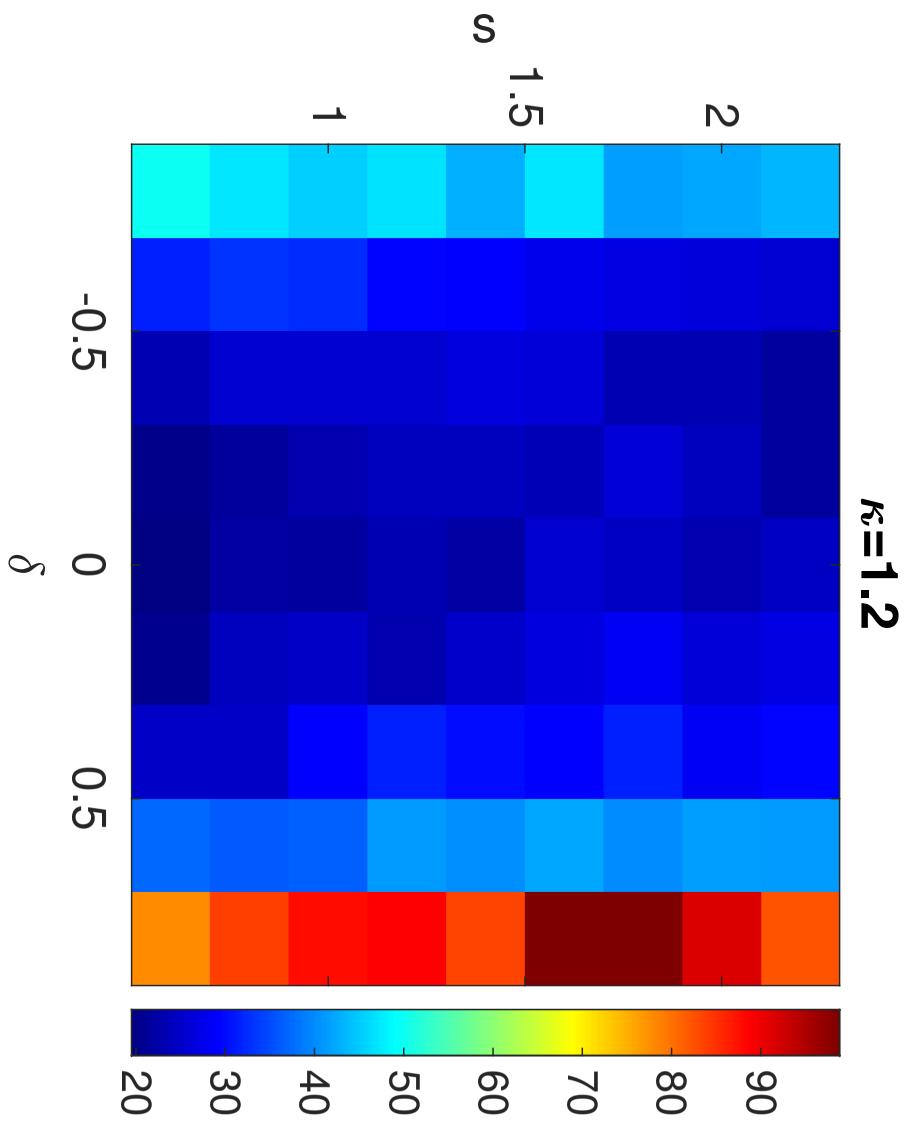

Physics of Plasmas

PLEASE CITE THIS ARTICLE AS DOI: 10.1063/5.0167292

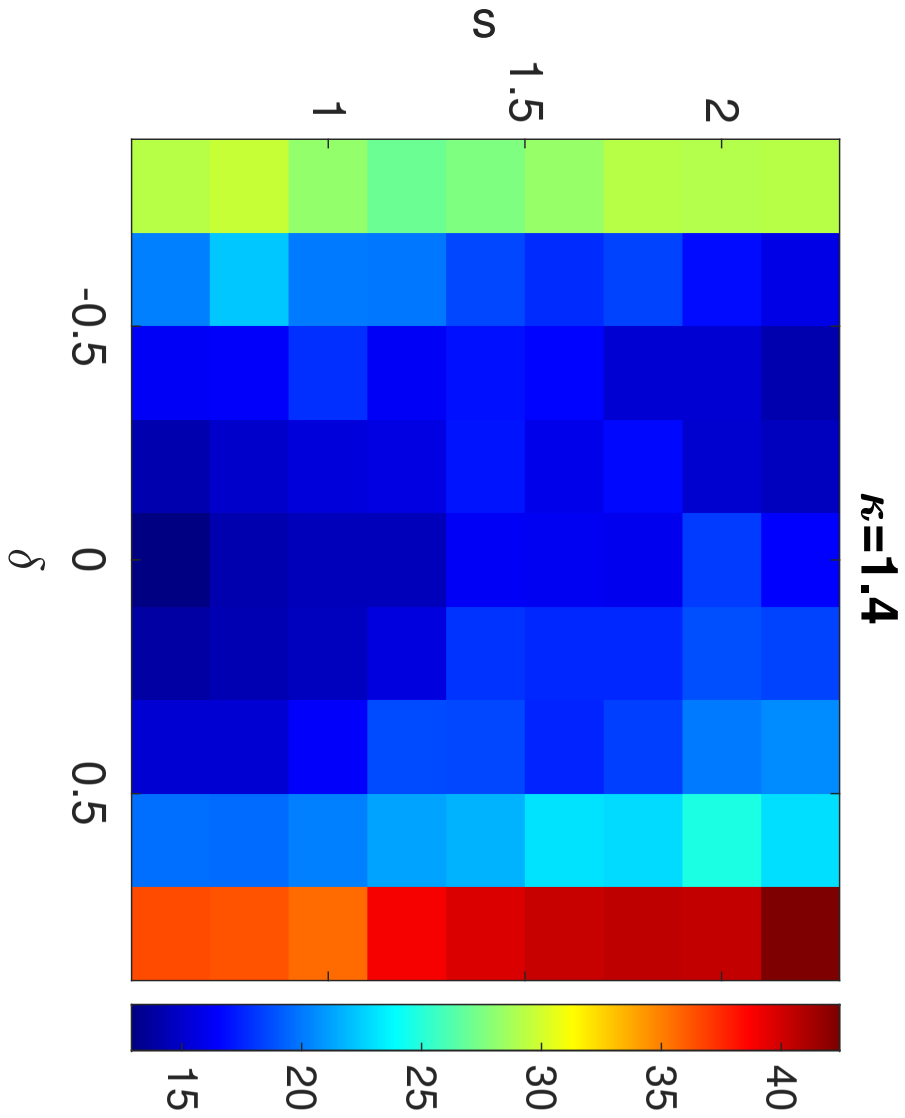

Physics of Plasmas

PLEASE CITE THIS ARTICLE AS DOI: 10.1063/5.0167292

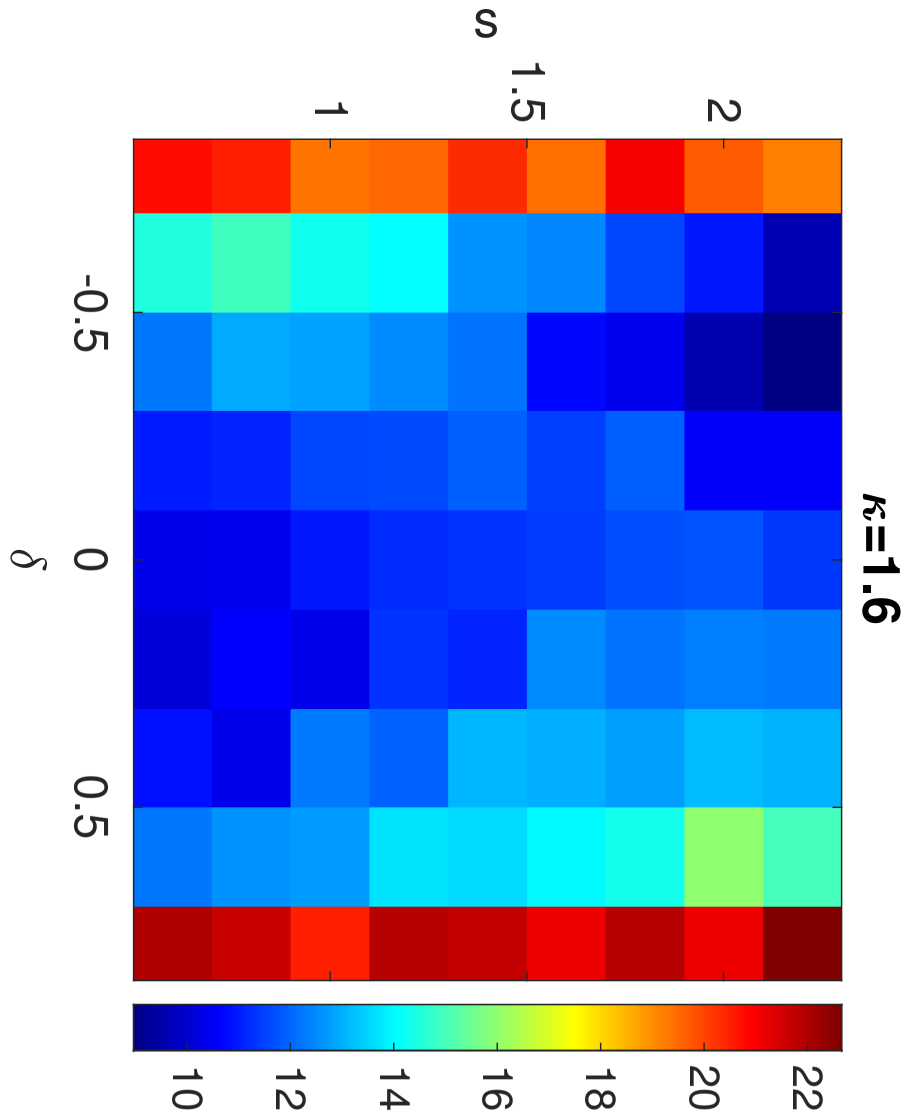

PLEASE CITE THIS ARTICLE AS DOI: 10.1063/5.0167292

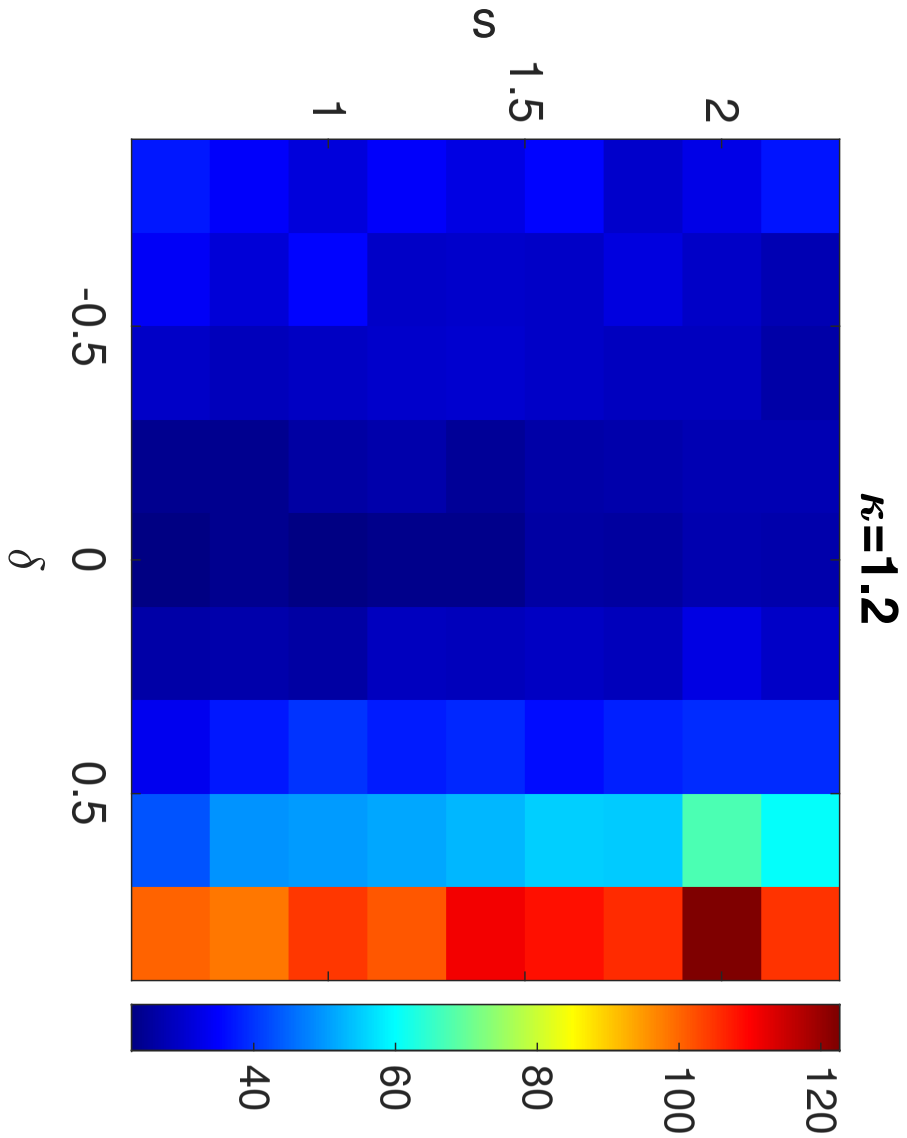

PLEASE CITE THIS ARTICLE AS DOI: 10.1063/5.0167292

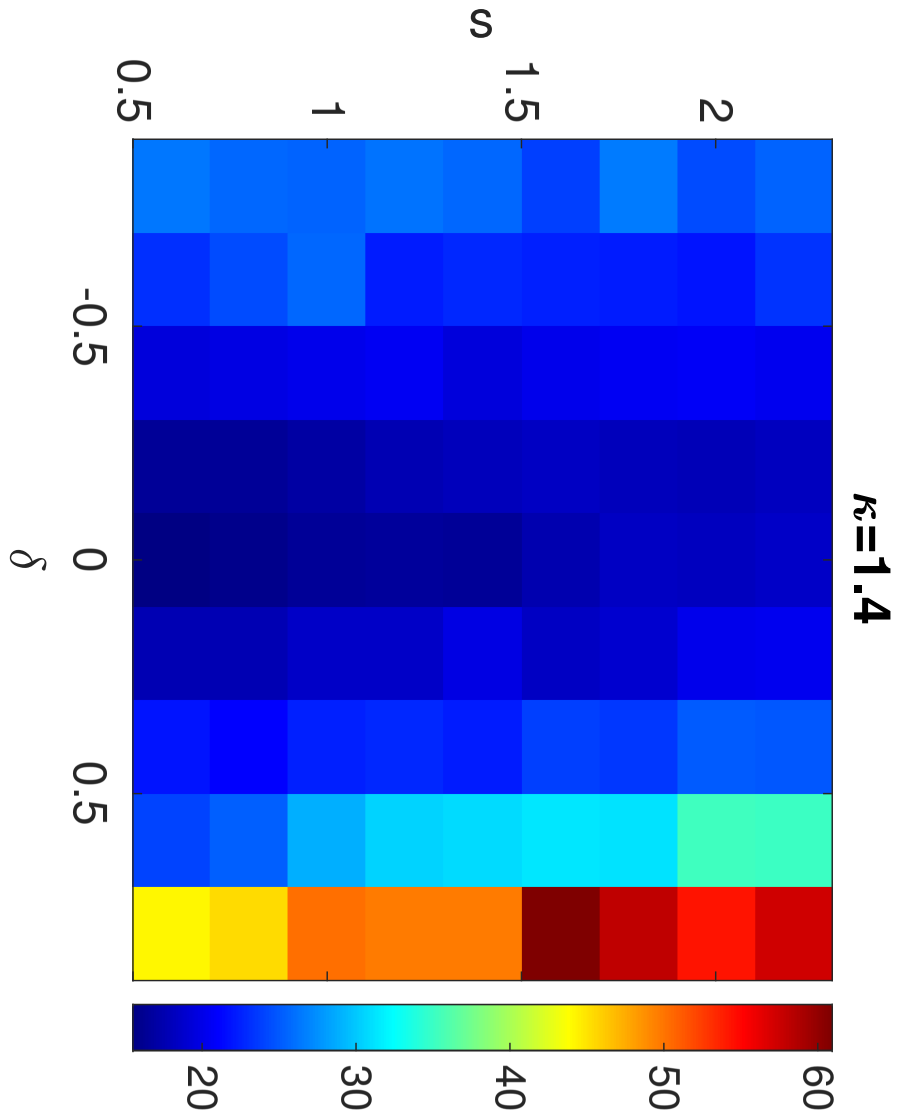

Physics of Plasmas

PLEASE CITE THIS ARTICLE AS DOI: 10.1063/5.0167292

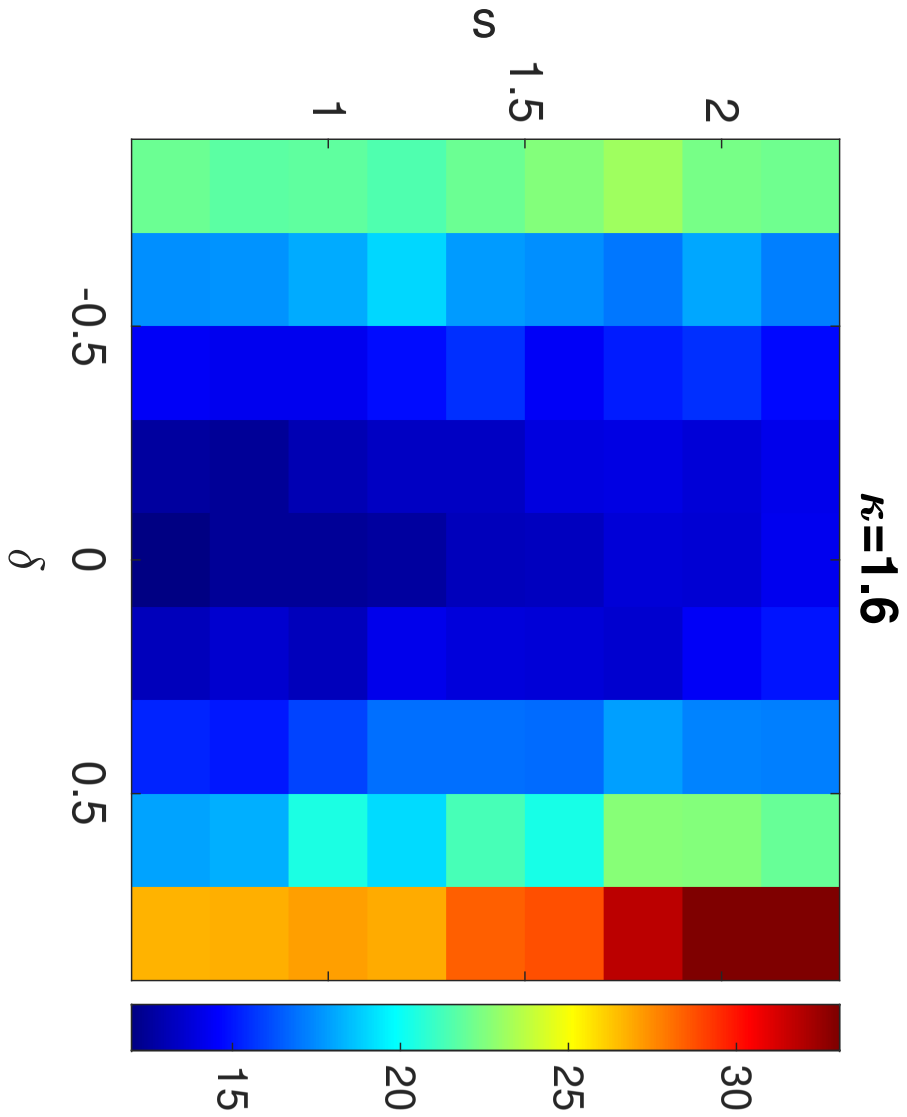

PLEASE CITE THIS ARTICLE AS DOI: 10.1063/5.0167292

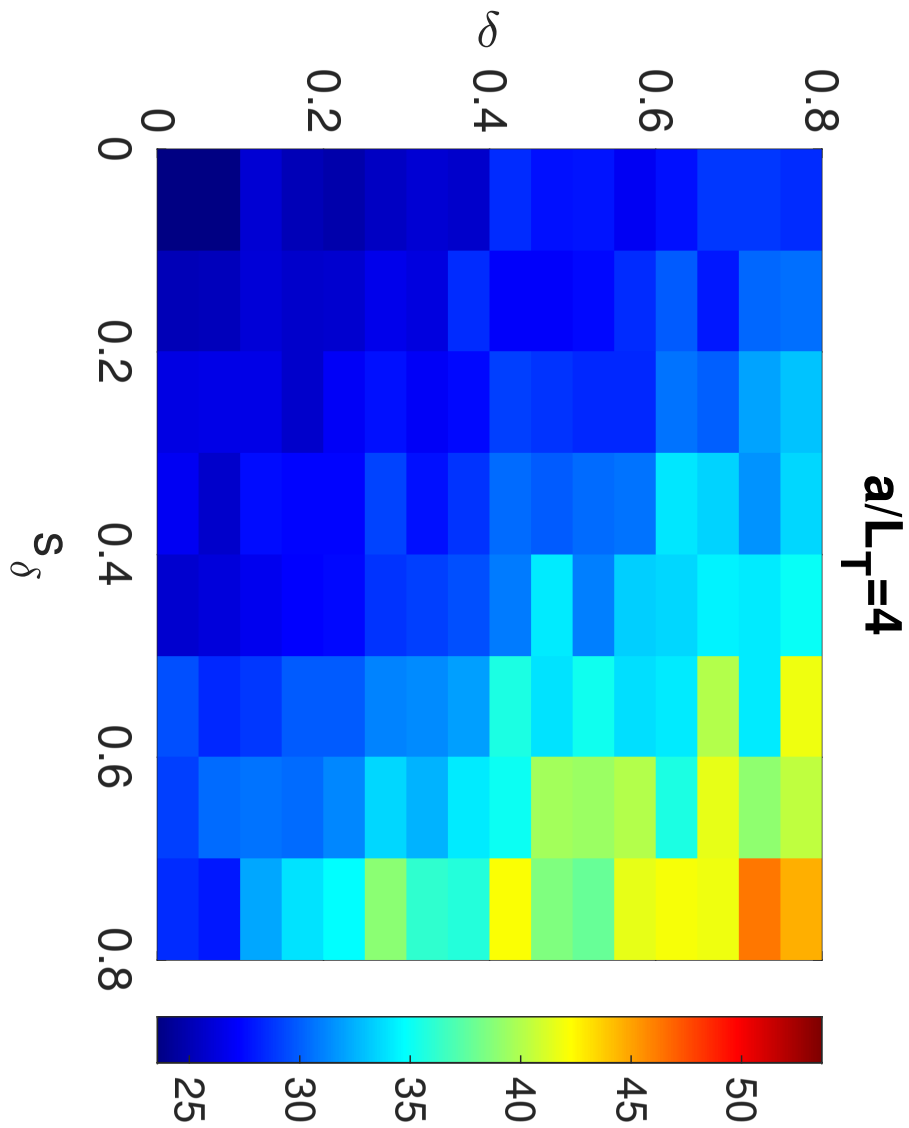

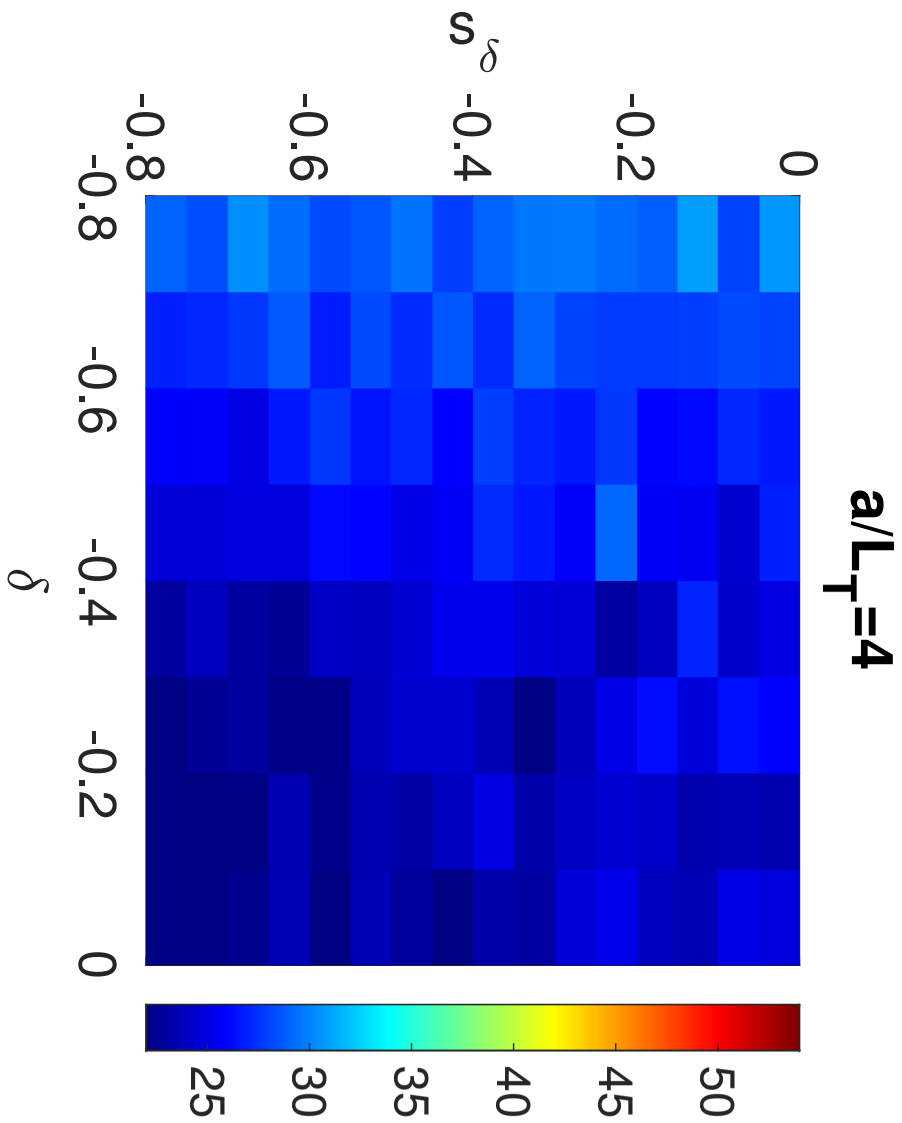

PLEASE CITE THIS ARTICLE AS DOI: 10.1063/5.0167292